Exploring the advantages of multiband fMRI with simultaneous EEG to investigate coupling between gamma frequency neural activity and the BOLD response in humans.

Makoto Uji[a], Ross Wilson[a], Susan T. Francis[b], Karen J. Mullinger[a,b]*†, Stephen D. Mayhew[a]*

[a] Centre for Human Brain Health (CHBH), School of Psychology, University of Birmingham, Birmingham, UK

[b] Sir Peter Mansfield Imaging Centre (SPMIC), School of Physics and Astronomy, University of Nottingham, Nottingham, UK

* these authors were equally responsible for leading this study

† corresponding author

Abstract

We established an optimal combination of EEG recording during sparse multiband (MB) fMRI that preserves high resolution, whole brain fMRI coverage whilst enabling broad-band EEG recordings which are uncorrupted by MRI gradient artefacts (GAs). We firstly determined the safety of simultaneous EEG recording during MB fMRI. Application of MB factor=4 produced <1°C peak heating of electrode/hardware during 20-minutes of GE-EPI data acquisition. However, higher SAR sequences require specific safety testing, with greater heating observed using PCASL with MB factor=4. Heating was greatest in the electrocardiogram channel, likely due to it possessing longest lead length. We investigated the effect of MB factor on the temporal signal to noise ratio for a range of GE-EPI sequences (varying MB factor and temporal interval between slice acquisitions). We found that, for our experimental purpose, the optimal acquisition was achieved with MB factor=3, 3mm isotropic voxels and 33 slices providing whole head coverage. This sequence afforded a 2.25s duration quiet period (without GAs) in every 3s TR. Using this sequence we demonstrated the ability to record gamma frequency (>55-80Hz) EEG oscillations, in response to right index finger abduction, that are usually obscured by GAs during continuous fMRI data acquisition. In this novel application of EEG-MB fMRI to a motor task we observed a positive correlation between gamma and BOLD responses in bilateral motor regions. These findings support and extend previous work regarding coupling between neural and haemodynamic measures of brain activity in humans and showcase the utility of EEG-MB fMRI for future investigations.

Keywords

EEG-fMRI
Multiband or multislice fMRI
Gamma-BOLD coupling
Gradient artefacts
Safety
Heating
Motor gamma oscillations

Introduction

Electroencephalography (EEG) and functional magnetic resonance imaging (fMRI) are two neuroimaging techniques that are often used to investigate human brain function. Simultaneous EEG-fMRI recordings provide a wide range of complimentary information and can be advantageous for improving our understanding of brain function, for example: through investigating the spatiotemporal dynamics of neural activity (for a review, see Huster et al., 2012), or studying the underlying neurophysiological origins of the measured responses by comparing neural and haemodynamic signals e.g. (Mullinger et al., 2013). The primary advantage of simultaneous EEG-fMRI acquisition over separate recordings is that it enables investigation of unpredictable or spontaneous brain activity, as well as studying the trial-by-trial covariation in brain processing as measured by the two techniques (Bagshaw et al., 2004; Becker et al., 2011; Debener et al., 2006; Eichele et al., 2008; Goldman et al., 2002; Horovitz et al., 2008; Mayhew et al., 2013; Mobascher et al., 2009; Mullinger et al., 2014; Olbrich et al., 2009; Scheibe et al., 2010). Thus simultaneous recordings enable spatial localisation of temporally dynamic response features. EEG-fMRI analysis has provided many novel insights into brain function. For example, such analyses have demonstrated specific BOLD correlates of: distinct neurophysiological components including the auditory oddball (Bénar et al., 2007; Eichele et al., 2005) and the error-related negativity (Debener et al., 2005); as well as specific neural activity in specific frequency bands (Goldman et al., 2002; Laufs et al., 2003). These studies have shown that simultaneous EEG-fMRI can provide greater specificity regarding the spatial arrangement (Goldman et al., 2009; Novitskiy et al., 2011) or the temporal sequence (Eichele et al., 2005; Mayhew et al., 2012) of responsive brain areas, compared to that revealed by a standard analysis of data from a single neuroimaging modality.

Recently, neuronal activity in the gamma frequency band, which is typically defined as between approximately 30-100Hz, has attracted much interest because gamma synchronization

has been linked with a range of cognitive and sensory functions (Buschman and Miller, 2007; Buzsaki and Draguhn, 2004; Colgin et al., 2009; Fries, 2009; Singer and Gray, 1995). Gamma-band synchronization has been observed in humans using non-invasive imaging methods during visual (Hoogenboom et al., 2006; Muthukumaraswamy and Singh, 2013), somatosensory (Bauer et al., 2006) and auditory (Pantev et al., 1991; Schadow et al., 2009) stimulation. It is also known to be involved in higher cognitive functions such as memory processes (Fell et al., 2001; Howard et al., 2003) and motor control (Brown et al., 1998; Cheyne et al., 2008; Crone et al., 1998; Darvas et al., 2010; Gaetz et al., 2010; Muthukumaraswamy, 2010; Schoffelen et al., 2005). Therefore, due to the functional importance of gamma frequency activity, characterising the underlying mechanisms of these responses is of great interest.

The majority of previous work investigating the link between BOLD signals and gamma activity has been conducted using invasive electrode recordings of local-field potentials in humans (Mukamel et al., 2005; Murta et al., 2016; Nir et al., 2007), primates (Logothetis et al., 2001; Magri et al., 2012; Niessing et al., 2005; Scholvinck et al., 2010; Viswanathan and Freeman, 2007) and rodents (Boorman et al., 2015; Sumiyoshi et al., 2012). These studies showed the BOLD response is more strongly coupled to gamma frequency activity, compared with the activity in the lower (<30Hz) frequency bands.

Whilst providing novel insights into neurovascular coupling, findings from invasive animal recordings cannot be easily extrapolated to scalp electrophysiological recordings due to differences in the recording references used and in the spatial scale of the neuronal populations involved in generating the signals (Hall et al., 2005). In addition, although the coupling between BOLD and gamma-LFP activity is widely cited as principle evidence for the neural underpinnings of haemodynamic based functional neuroimaging, the majority of these seminal studies have been conducted in visual cortex (Logothetis et al., 2001; Viswanathan and Freeman, 2007), with some exceptions in auditory cortex (Mukamel et al., 2005). A wider

understanding in other brain regions, for example sensorimotor cortex, is important to fully establish the fundamental nature of the gamma-BOLD relationship. Such investigations are particularly important given the recent doubt cast on the functional importance of narrow-band gamma responses in visual cortex (Hermes et al., 2014), and the BOLD correlates of broader high-frequency activity (Winawer et al., 2013). Therefore non-invasive simultaneous EEG-fMRI recordings in humans offer many potential advantages for relating gamma and BOLD signals. Possibilities include extending previous studies suggestions of a strong gamma-BOLD relationship by investigating this coupling in motor paradigms, which have been widely shown to induce robust increases in gamma power (Cheyne et al., 2008; Crone et al., 1998; Gaetz et al., 2010; Muthukumaraswamy, 2010) , and gaining a fuller understanding of the fundamental relationship of these signals to each other and also to human behaviour (Hoogenboom et al., 2010; Womelsdorf et al., 2006).

However, few simultaneous EEG-fMRI studies have investigated gamma activity due to technical limitations as detailed below, and consequently the relationship between haemodynamic responses and the gamma band activity in humans remains incompletely understood (Logothetis, 2008). The recording of EEG data in the MRI environment is technically challenging primarily due to the effect of the MRI on the EEG data quality. Namely, EEG data are corrupted by the gradient artefact (GA) produced by the time-varying magnetic field gradients needed for imaging, the pulse artefact produced by cardiac pulse driven motion in the strong magnetic field of the MR scanner, and motion artefacts due to head movement in the MR environment (Mullinger and Bowtell, 2011). The frequency characteristics of these artefacts mean that the GA is the primary problem for studying gamma band activity, with residual GAs easily obscuring the small amplitude neuronal signal of interest even after correction (Mullinger et al., 2011, 2008b).

Despite the technical challenges, a few studies have attempted to study the gamma band using concurrent EEG and fMRI measures (Castelhano et al., 2014; Green et al., 2017; Leicht et al., 2016; Mantini et al., 2007; Michels et al., 2010; Mulert et al., 2010; Rosa et al., 2010; Scheeringa et al., 2011). Of these a number limited the frequency range of the measured gamma band to a range of 30-50Hz (or narrower) to avoid the high frequencies where the GAs dominate (e.g. Mantini et al., 2007; Mulert et al., 2010; Rosa et al., 2010). However, this band limiting approach, is clearly suboptimal when gamma responses that are often reported in the upper portion of the 30-100 Hz frequency range (Muthukumaraswamy, 2010) have been related to behaviour and other neuronal measures e.g. GABA concentration (Muthukumaraswamy et al., 2009). An alternative approach taken by other studies, or in addition to band-limiting gamma, has been to adopt a sparse fMRI sequence (Leicht et al., 2016; Mulert et al., 2010; Scheeringa et al., 2011) rather than conventional, continuous fMRI acquisition. Sparse sequences feature an acquisition time shorter than the repetition time (TR) of the MRI sequence in order to provide a time window with no MRI gradients present in which to collect EEG data. As a result this approach enables the full gamma frequency range to be investigated. However, conventional MRI sequences require a long TR (>3s) and/or small number of slices to be acquired to provide the required sparsity; imposing limitations in the temporal sampling or spatial coverage possible and consequently limiting the utility of the fMRI data acquired.

Therefore in order to optimize simultaneous EEG-fMRI recordings to study gamma-BOLD coupling, we need to establish a novel method to obtain cleaner EEG data in the high (>30Hz) frequency band. Multiband (MB) fMRI has the potential to overcome the limitations imposed by conventional sparse fMRI sequences. MB acquisition (Feinberg et al., 2010; Moeller et al., 2010) can be employed to: shorten repetition times (TR); increase brain coverage for a given TR; or shorten the acquisition time of whole-head fMRI in a sparse fMRI sequence which would lengthen the gradient-free time window in which EEG data can be collected. Sparse MB

fMRI acquisitions therefore offer great potential for improving EEG data quality during simultaneous acquisitions. However, due to the additional radio frequency (RF) power of MB excitation the safety of EEG-MB fMRI acquisitions must be assessed (Auerbach et al., 2013). In addition, as MB methods can affect temporal signal to noise (tSNR) of fMRI data (Chen et al., 2015; Todd et al., 2016) assessing the implementation of MB and the effect on fMRI tSNR is also important to enable optimised EEG-fMRI studies to take place.

Therefore the aim of this work was to assess the overall feasibility of recording EEG simultaneously with MB fMRI in humans. This took place in three parts: i) assessing the safety implications of EEG-MB fMRI; ii) assessing the tSNR of MB fMRI and iii) applying an optimised EEG-MB fMRI approach to investigate single-trial coupling relationships between MB-BOLD and gamma and beta frequency EEG responses to a finger-abduction motor task. We chose to investigate motor responses as an event-related synchronisation (ERS) of gamma oscillations (reflecting an increase in power), typically accompanied by desynchronization (ERD) of beta frequency (15-30Hz) oscillations (reflecting a reduction in power), in the primary motor cortex contralateral to the movement have been well documented using invasive electroencephalography (ECoG) (Darvas et al., 2010), MEG (Muthukumaraswamy, 2010) and EEG (Cheyne et al., 2008) (for reviews, Cheyne and Ferrari, 2013; Cheyne, 2013; Muthukumaraswamy, 2013). To our knowledge, the motor gamma-BOLD relationship has not previously been investigated with simultaneous EEG-fMRI acquisition in humans. Therefore, through this proof of concept study we also aim to widen the understanding of gamma-BOLD coupling across the cortex. We hypothesise that the single-trial positive BOLD response in contralateral motor cortex will correlate positively with gamma power ERS and negatively with beta power ERD.

Methods

Data were acquired and analysed in two stages. Stage one consisted of initial safety testing and image-quality optimisation of EEG-MB fMRI; whilst stage two involved the application of the optimised scanning protocol for the concurrent EEG-fMRI study of human brain responses during motor tasks.

During both stages, EEG data were acquired using BrainAmp MRplus EEG amplifiers (Brain Products, Munich) with 5kHz sampling rate and an MR-compatible 63-channel EEG cap (EasyCap, Herrsching). The hardware band-pass filters were set to a 0.016-250 Hz range, with a roll-off of 30 dB/octave at high frequency. Electrode layout followed the extended international 10-20 system with an additional channel for recording the electrocardiogram (ECG). FCz was used as the reference electrode. A 3T Philips Achieva MRI scanner with a body transmit and 32-channel receiver-array head coil was used for MR data acquisition. The MB implementation for fMRI acquisitions in this study was from Gyrotools, Zurich. MR-EEG scanner clocks were synchronised for all EEG data acquisition (Mullinger et al., 2008b). All data acquisition on humans was performed with approval from the local ethics committee and informed consent was obtained from all subjects involved in this project.

Stage 1: Assessing the safety and tSNR of EEG-MB fMRI

Safety testing

Safety testing was performed on a conductive, head shaped phantom with a conductivity of about $0.5\Omega^{-1}m^{-1}$ to mimic skin conductivity (Yan et al., 2010). The phantom was left in the scanner room over night to equilibrate to the ambient temperature. The EEG cap was then connected to the phantom using conductive gel (Abralyte 2000 [EasyCap GmbH, Munich]) and all electrode impedances were maintained below 15kΩ. Fibre-optic thermometers (Luxtron

Corporation, Santa Clara, CA, USA) were used to continually monitor (1 Hz sampling rate) heating effects at seven locations: four scalp electrodes (Cz, TP7, FCz & TP8), the ECG lead (connected to the base of the phantom's neck), the cable bundle coming from the EEG cap and the scanner bore (as a control measurement of heating effects unrelated to the presence of the EEG system). Thermometer sensors were placed in the conductive gel under the electrodes and taped to the surface of the cable bundle and scanner bore. The phantom was then placed at the MR scanner iso-centre. Firstly, a 5-minute recording of baseline temperature at each location was collected without any scanning. Then two 20-minute MRI scans, both employing MB factor 4 and spectral presaturation with inversion recovery (SPIR) fat suppression, were performed to test for heating during the highest realistic values of specific absorption rate (SAR) for a given sequence type. Please note MB factor 4 was the highest available in this implementation of MB. The sequences tested were: 1) gradient echo (GE)-EPI (using: TR/TE=1000/40ms, SENSE=2, slices=48, B1 RMS=1.09μT, SAR/head=22%); 2) Pseudo-continuous arterial spin labelling (PCASL)-GE-EPI (using: TR/TE=3500/9.8ms, SENSE=2, slices=32, B1 RMS=1.58μT, SAR/head=46%). Between the two MRI scans there was a 10 minute period without scanning to allow a return to baseline following any heating effects from the previous MRI scan.

Analysis

The mean baseline temperature at each thermometer location was determined using the 5 minute recording prior to each MRI scan. For each location, the mean baseline temperature was then subtracted from the temperature timeseries recorded during each scan to give the change in temperature across the whole 20 minute scan period.

Image quality: tSNR

To assess the effect of the implementation of MB excitation on the fMRI signal tSNR, fMRI data were recorded on 3 healthy-adult subjects (age 32 ± 2 years) during five different GE-EPI pulse sequences:

i) MB factor = 1 with equidistant slice acquisition

ii) MB factor = 2 with equidistant slice acquisition

iii) MB factor = 2 with sparse slice acquisition

iv) MB factor = 3 with equidistant slice acquisition

v) MB factor = 3 with sparse slice acquisition

Equidistant acquisition used the full TR period, comprised of equal temporal intervals between each slice acquisition. For sparse acquisitions MR data were acquired in the minimum possible time at the beginning of the TR period; the rest of the TR period then formed a quiet period with no MR gradients. A TR = 3060ms and 36 slices were chosen to ensure that these parameters could be used for all combinations of MB factors and slice acquisition (in scans i-v) whilst adhering to requirements for EEG clock synchronisation (Mandelkow et al., 2006; Mullinger et al., 2008b). Other parameters were set for all scans as follows: TE= 40ms, SENSE=2, flip angle=79°, 41 volumes acquired. A T1-weighted anatomical image was also acquired for each subject.

Analysis

For each subject the anatomical image was used to segment the grey matter (FSL FAST, https://fsl.fmrib.ox.ac.uk/fsl/) (Zhang et al., 2001) which formed a mask for subsequent analysis. The tSNR was calculated in every grey matter voxel (Eq. 1) and then averaged over voxels for each subject. The group mean and standard deviation in grey matter of the tSNR was then found for each of the five scans to assess the change in tSNR with MB factor and slice acquisition scheme.

$$tSNR_{voxel} = \frac{mean\ signal\ over\ time_{voxel}}{standard\ deviation\ over\ time_{voxel}}$$

Eq. 1

Stage 2: EEG-fMRI motor study

12 right-handed subjects (10 males, 2 females, age = 26.6 ±5.7) took part in the study. After initial data processing, two subjects were excluded from further analysis due to repeated, excessive head motion (>4mm, as assessed from fMRI realignment parameters).

Data acquisition

The EEG cap was put on the subject and all electrode impedances were maintained below 10kΩ for the duration of the study. EEG-fMRI data were acquired using a sparse GE-EPI scheme (TR=3000ms (of which: acquisition time=750ms, quiet period=2250ms), TE=40ms, MB factor=3, 33 slices, voxels=3mm^3, SENSE = 2, FOV = 240 x 240 mm, flip angle = 79°, 192 volumes, SAR/head<7%). These parameters had been optimised based on the results of Stage 1 and the requirements of the paradigm (see below). High frequency (>30 Hz) artefacts were minimised by mechanically isolating the EEG amplifiers from the scanner bed and minimising MR scanner room environment noise (Mullinger et al., 2013; Mullinger and Bowtell, 2011). In addition, the subject was positioned such that electrodes Fp1 and Fp2 were at the iso-centre in the foot/head direction so as to further reduce the amplitude of the GAs (Mullinger et al., 2011). Foam padding was placed around the subject's head to reduce motion-related artefacts. The EEG and MR scanner clocks were synchronised (Brain Products Synchbox), and the TR made equal to a multiple of the EEG sampling period, to ensure consistent sampling of the GA waveforms (Mandelkow et al., 2006; Mullinger et al., 2008b). The onset of every TR period was marked in the EEG data to facilitate GA correction. Simultaneous electromyogram (EMG) recordings were made from electrodes attached over the first dorsal interosseous (FDI) muscle

of the right hand using a Brain Product EXG amplifier. Cardiac and respiratory cycles were simultaneously recorded using the scanner's physiological monitoring system (vector cardiogram (VCG) and respiratory belt). A T1-weighted anatomical image (MPRAGE sequence) with 1mm isotropic resolution was also acquired. EEG electrode locations were digitised (Polhemus Fastrak) to facilitate individualised co-registration of electrode positions with each subject's anatomical image.

Paradigm

Subjects performed abduction movements of the right-hand index finger in time with an auditory cue (1 kHz tones, 50ms duration, 2.5Hz presentation rate) that was delivered to both ears via headphones, as previously employed in an MEG study (Muthukumaraswamy, 2010). A single trial consisted of four abduction movements which were performed briskly following each auditory cue within the MR gradient quiet period of a single TR. The onset of the first cue was 250ms after the end of the MR acquisition in that TR, such that the cues occurred at 1000, 1400, 1800 and 2200ms relative to the start of a given TR, resulting in all movements occurring within a 1.5s window for each trial. Abduction trials were separated by a 16s (five 3s TR periods + 750ms MR acquisition + 250ms) resting baseline interval (see Figure 1). Subjects were instructed to fixate on a centrally displayed cross, to keep their hands by their sides and to remain as still as possible throughout the whole experiment. Immediately prior to the first auditory cue of each trial, a visual cue appeared, the fixation cross changed to a plus sign for 2s, warning the subjects to prepare for the upcoming trial. Subjects performed a 10-minute practice outside the scanner (50 trials of the same auditory cued abduction task for 1.5s, separated by an interval of 5.5s and EEG recorded) in order to familiarize themselves with the

paradigm and were then subsequently positioned inside the MRI scanner where they each completed four runs of 30 trials during fMRI, resulting in 120 trials per subject in total.

Analysis

EEG

Cardiac R-peaks were detected from the VCG recording and used to inform pulse artefact correction of data recording inside the scanner (Mullinger et al., 2008b). For both EEG and EMG data, gradient and pulse artefacts were corrected in BrainVision Analyzer2 using sliding window templates formed from the averages of 45 and 21 artefacts respectively, which were subtracted from each occurrence of the respective artefacts. Data were subsequently downsampled (600Hz), bandpass filtered (EEG: 0.5-120Hz, EMG: 0.5-45Hz) and epoched into single-trials from -16s to 2s relative to the onset of the first auditory cue in each trial (BrainVision Analyzer2). Through visual inspection of the data, noisy EEG channels and trials that were contaminated with large motion artefacts, substantial EMG activity during the baseline period, or showed a lack of abduction movement in the EMG signal, were removed. This resulted in a group mean (±standard error [SE]) of 84 ± 2 trials remaining for further analysis. Independent component analysis of the EEG data (ICA, EEGLAB, https://sccn.ucsd.edu/eeglab/) was then used to remove eye-blinks/movements (Delorme and Makeig, 2004; Jung et al., 2000), with an average of 2 ICs (SE = 1) removed per subject, and data were re-referenced to an average of all non-noisy channels.

Individual, 4-layer (scalp, skull, CSF, & brain) boundary element (BEM) head models were constructed from the T1 anatomical image of each subject using the Fieldtrip toolbox (http://www.ru.nl/neuroimaging/fieldtrip) (Oostenveld et al., 2011). A Linearly Constrained Minimum Variance (LCMV) beamformer (Robinson and Vrba, 1999; van Drongelen et al., 1996; van Veen et al., 1997) was then employed to separately spatially localise changes in each

subject's gamma (55–80Hz) and beta (15-30Hz) frequency oscillations (filtered using 2nd order Butterworth filters) in response to abduction movements. The optimal frequency band for the localisation of gamma ERS was determined based on an iterative process of initially investigating time-frequency spectrograms created from broad gamma band (30-100Hz) source localisation and observing that consistently, across subjects, the peak gamma ERS was found in the 55-80Hz, gamma band range, in agreement with many previous findings (Ball et al., 2008; Cheyne et al., 2008; Muthukumaraswamy, 2010; for reviews, Cheyne and Ferrari, 2013; Cheyne, 2013; Muthukumaraswamy, 2013). For each subject and frequency band (beta or gamma), source power during the active (0s to 1.5s) and passive (-9.0s to -7.5s) time windows, defined relative to the first cue onset, were calculated. The passive window definition in the baseline interval, during the first MR-quiet period that preceded the visual probe cue of that trial, was chosen to avoid both the periods of MR acquisition and any brain activity occurring due to the visual cue. Subsequently, pseudo T-statistic (Ŧ-statistic) maps were computed as the ratio of the difference in source power between the active and passive windows, divided by the sum of the noise power estimates inherent to the sensors during both active and passive windows (Hillebrand and Barnes, 2005; Robinson and Vrba, 1999).

The maximum peak Ŧ-statistic location of the gamma power ERS and minimum peak Ŧ-statistic location of the beta power ERD in the contralateral primary motor cortex (cM1) defined the site of a gamma and a beta virtual electrode (VE). A broadband (1-120Hz) timecourse of neural activity was then extracted from these two VE locations, by multiplying the channel level data by the respective broadband beamformer weights. Time-frequency spectrograms of gamma and beta VE data were calculated using a multitaper wavelet approach (Scheeringa et al., 2011). Windows of 0.4s duration were moved across the data in steps of 50ms, resulting in a frequency resolution of 2.5Hz, and the use of seven tapers resulted in a spectral smoothing of ±10Hz. Using the mean of the passive window data as baseline the

spectrograms were converted to display change in activity relative to baseline. Separately for each subject, VE timecourses were filtered into the gamma and beta bands, Hilbert transformed and then the average power during the active window was calculated for each trial (Mayhew et al., 2010; Mullinger et al., 2014). These single trial power values were then mean-subtracted to form regressors of gamma and beta power, which represented the trial-by-trial variability in single-trial stimulus response amplitudes, for subsequent GLM analysis of fMRI data. The amplitude of rejected trials was set to the mean value (zero). EEG data recorded outside the scanner were analysed using equivalent methodology, to provide comparison of data quality with the inside scanner recordings.

fMRI

fMRI data were processed using FSL v5.0.9 (https://fsl.fmrib.ox.ac.uk/fsl/). Data from each subject were motion corrected (MCFLIRT), spatially smoothed (5mm FWHM Gaussian kernel), high-pass temporally filtered (100s cutoff), registered to their T1 anatomical brain image (FLIRT), and normalised to the MNI 2mm standard brain. GLM analyses were performed using FEAT v6.0. First-level analysis was performed employing four regressors: 1) boxcar abduction movement, 2) boxcar visual probe cue, 3&4) parametric modulation of single-trial gamma and beta neuronal responses, respectively. All regressors were convolved with the double-gamma HRF. Both positive and negative contrasts were assessed for each regressor. For each subject and frequency band, first-level results were combined across all four runs using a second-level, fixed effects analysis to calculate an average response per subject. These results were then combined across all subjects at the third, group-level using a FLAME mixed-effects analysis (Woolrich et al., 2004). Since our a-priori hypothesis was to investigate motor fMRI responses and their correlation with gamma and beta EEG activity, a

mask of motor cortex (Oxford–Harvard cortical atlas, FSL) was applied as pre-threshold mask to all group-level statistical maps before cluster correction. Main effect (boxcar model of the task) and the single trial EEG regressor correlation BOLD Z-statistic images were threshold using $Z > 2.3$ and cluster corrected significance threshold of $p < 0.05$.

Results

Stage 1: Feasibility testing

Safety testing

The temperature changes measured at all thermometer sensors during the GE-EPI sequence are plotted in Figure 2. The greatest heating was observed in the ECG channel, which showed a ~0.5°C increase. This temperature increase occurred gradually over the first 10 minutes and then stabilised and showed no further change. Nominal heating was observed in the other channels. The higher SAR of the PCASL sequence resulted in a greater heating effect than the GE-EPI, again the largest temperature increase was seen in the ECG channel (~0.9°C) with increases in other channels (TP8 = ~0.8°C) also observed (Supporting Information, Figure S1). As this GE-EPI sequence, with parameters chosen to maximise SAR, showed no heating effect close to 1°C, the use of the MB GE-EPI (with parameters resulting in lower SAR) with the EEG system was regarded safe for the following experiments (Carmichael et al., 2008; Medicines and Healthcare Products Regulatory Agency, 2015).

Image quality: tSNR

The variation in BOLD tSNR with MB factor = 1-3 and slice spacing acquisition is summarised in Table 1. These data indicate that the variability in tSNR between subjects was far larger than

the variability of tSNR with imaging parameters. Figure 3 shows the spatial variation in tSNR over a single slice for each subject for the two sparse imaging acquisition sequences tested, which were the most promising sequences for our EEG-fMRI application. Visual inspection of the images in Figure 3 and direct comparison of the mean and standard deviation of tSNR within subjects shows no clear change in tSNR (12.6 ± 22% between MB factor 2 to 3) between MB factors. Since, for sparse sequences, using a MB factor of 3 compared with 2 results in a 33% reduction in the time required to acquire the same number of slices the MB factor of 3 was chosen for the EEG-fMRI experiment, to maximise the duration of the MR quiet-period for EEG measurements without degradation of the tSNR.

Study 2: ***EEG-fMRI motor study***

All subjects performed the abduction task as instructed, judged by visual inspection of the EMG data showing increases in power during brisk finger movements which accurately timed to the auditory cues, and EMG power returning to rest levels during the baseline periods showing subjects remained still in these periods. Mean rectified EMG activity during the passive and active periods is shown for a representative subject in Figure 4.

Figure 5 shows the group average T-statistic map of changes in both EEG gamma- and beta-power during the active window compared to the passive window. An increase in gamma power (ERS, positive T values, Fig. 5a) was only observed in contralateral M1, whereas a decrease in beta power (ERD, negative T values, Fig. 5b) was observed in bilaterally in contralateral and ipsilateral M1. Specifically, the mean of the individual subject VE locations in cM1 for the gamma ERS was found at: [-21±3, -31±3, 59±3] mm *[MNI:x,y,z]* (see Fig 5a, crosshair) and the beta ERD was found at [-39±3, -32±2, 51±4] mm (see Fig 5b, crosshair), where errors denote standard error over subjects. Both these locations lie in the post-central

gyrus, the gamma VE location was found to be significantly more medial ($t(9) = 3.76$, $p=0.004$ paired t-test) than the beta VE location, but no difference in the y ($t(9) = 0.41$, $p=0.69$) or z ($t(9) = 1.32$, $p=0.21$) co-ordinates was observed.

Figure 6 shows the group mean time-frequency spectrograms measured from cM1 for the gamma (Fig 6a&b) and beta (Fig 6c&d) VE locations. Figures 6a&c display the mean time-frequency spectrogram for the whole 18s duration of the abduction trial and preceding inter-trial interval, with Figure 6b&d showing the active and passive periods only. The broadband increases in power (red vertical stripes lasting ~750ms and occurring every 3s) show the effect of the residual GAs caused by the MRI data acquisition on the EEG power spectrum. It is clear that neuronal EEG responses above 20 Hz recorded during MRI data acquisition are corrupted by residual GAs with signal degradation increasing with increasing frequency (Fig. 6a&c). Note that, due to the way the trials were epoched, the increase in <30Hz power between -16s and -14s represents the post-movement alpha/beta rebound. By selecting the active (0 to 1.5s) and passive (-9 to -7.5s) time windows during MR quiet periods a reliable comparison of neuronal signals between rest and task was made for both the gamma and beta bands (Fig. 6b&d). During the active window, when the FDI abduction movements were performed, ERS of gamma band power (55-80Hz) and ERD of beta band power (15-30Hz) occurred compared with the passive window of baseline resting fixation with no movement (Fig. 6b&d). As expected due to the VE definition, stronger gamma power ERS was observed in the gamma VE than the beta VE, and stronger beta power ERD was observed in the beta VE than in the gamma VE. Comparison of these results with those from data recorded outside the scanner (Supporting Information, Figures S2 and S3) shows that very similar gamma and beta responses were measured in both recordings, providing confidence in the quality of our data inside the scanner.

As expected across 10 subjects, we observed a significant main-effect (correlation with boxcar regressor) positive BOLD response to the abduction movements in the motor cortex, with the peak voxel ($Z=5.12$, $p<1x10^{-19}$) lying within the masked region found at [-38, -32, 66] mm *[MNI:x,y,z]* in cM1, as shown in Figure 7, red-orange. With a second peak ($Z=4.97$, $p<1x10^{-19}$) found on the midline at [-4, -14, 70] mm *[MNI:x,y,z]*. In addition a positive correlation between single-trial gamma power ERS and the BOLD response was observed in cM1, with the peak ($Z=3.11$, $p<0.001$) located at [-32, -42, 60] mm *[MNI:x,y,z]* (Fig 7, green) with additional responses in the ipsilateral primary motor cortex with the peak ($Z=3.02$, $p<0.01$) located at [34, -42, 60] mm *[MNI:x,y,z]* and on the midline with peak ($Z=2.97$, $p<0.01$) located at [2, -36, 56] mm [*MNI:x,y,z*]. No significant negative correlations were observed with the boxcar or gamma band regressors. No significant positive or negative correlations between single-trial beta and BOLD responses were observed.

Discussion

Here, through a series of experiments we show that, with the right safety precautions and MRI sequence choice, it is safe to simultaneously acquire EEG data with MB fMRI data, despite the higher peak RF power required for MB acquisitions compared with conventional fMRI acquisitions. We also show that, for the implementation of MB used here, there is no measurable degradation of the fMRI signal tSNR when moving to a sparse acquisition with a MB factor of 3 compared with the conventional continuous equi-spacing acquisition with no MB factor, allowing for the presence of physiological noise. We finally show the considerable gains that can be achieved in using MB fMRI with concurrent EEG data acquisition by studying gamma-BOLD coupling with a simple motor task. We were able to reliably detect the gamma response to finger abductions within cM1 and found that this response was positively correlated

with the BOLD response in bilateral primary motor cortex with activation extending directly posterior to the hand-knob area of the contralateral motor cortex.

Safety and signal quality considerations

We show that for a GE-EPI sequence using a MB factor of 4 resulting in a B1 RMS=1.09μT, SAR/head=22% that the maximum heating observed over a 20 minute period was ~0.5℃ (Figure 2) which is considerably less than the recommended 1℃ safety limit (Medicines and Healthcare Products Regulatory Agency, 2015). Furthermore the majority of this 0.5℃ temperature increase was observed within the first 5-6 minutes of scanning after which the temperature remained relatively constant suggesting that there is not a linear heating effect over time. Therefore even if data were continuously acquired for a longer period, which is uncommon in neuroimaging studies, the risk to the subject is unlikely to increase greatly. A similar pattern of heating was observed for the PCASL sequence where the greatest heating occurred in the first few minutes before a plateau was reached (Supporting Information, Figure S1). However, this heating effect was far greater, up to ~0.9℃ over the electrodes and locations measured, reflecting the increased B1 power used in that sequence (B1 RMS=1.58μT, SAR/head=46%). As this temperature rise was only just within the safe limit for human tissue (Medicines and Healthcare Products Regulatory Agency, 2015) and given that not all locations on the phantom were monitored, we would strongly suggest sequences such as MB-PCASL should not be used with concurrent EEG recordings. Although we didn't record temperature data from occipital electrodes due to practical limitations, we believe temperature increases at T7/T8 are likely to approximate the O1/O2 electrodes, due to similar wire lengths. The greatest heating effect in both GE-EPI and PCASL scans was observed in the ECG lead. This lead is considerably longer than the other leads in the EEG cap, which probably resulted in greater RF

absorption in this lead (Mullinger et al., 2008a) causing the larger heating effect observed here. Given the potential to use the VCG system, supplied by the MRI manufacturer, to monitor the cardiac cycle (Mullinger et al., 2008b) it would be possible to reduce the risk of heating effects by removing the ECG lead and electrode from the EEG setup. However, given the increase in temperature (~0.8℃) in the Tp8 electrode, which also has a relatively long lead, the removal of the ECG lead alone is unlikely to ensure that high SAR sequences can be run safely with EEG system present. These findings are in general agreement with recent work that also considered safety implication of MB (Foged et al., 2017). It is also important to note that minimal heating effects were observed at the MRI scanner bore location suggesting that the MR scanning was not increasing the ambient temperature of the bore. Therefore the observed electrode heating specifically arose from the interaction between the EEG system and the RF slice excitation pulses. These data highlight the potential dangers of using MB sequences for EEG-fMRI where high SAR values can arise from the increased B1 (Collins and Wang, 2011) and the need for specific safety testing of any sequences used. Since there are choices in how the RF pulses required for MB sequences can be implemented, with varying effects on SAR (Feinberg and Setsompop, 2013; Norris et al., 2011; Wong, 2012), it is important that MB implementations by different MR manufactures and software providers are individually tested before being used in human experiments.

It is known that the use of MB can reduce image quality and consequently degrade the temporal stability of the signals acquired using EPI based sequences (Chen et al., 2015; Todd et al., 2016). However, due to the ability of MB to shorten the TR, the increased temporal sampling can result in increased signal sensitivity per unit time as well as enhanced t-statistics of activation maps (Todd et al., 2016). MB fMRI has been shown to be useful in a number of different applications since its conception only a few years ago, with the relative gains in

sampling rate and voxel size that it can provide offsetting any signal quality degradation incurred (Boyacioğlu et al., 2015; Feinberg et al., 2010; Moeller et al., 2010; Olafsson et al., 2015). Indeed, our own investigations showed that the variation in tSNR over subjects was far greater than the variation in tSNR between the sequences tested with different MB factors and slice acquisition schemes (Table 1). This suggests that the tSNR measures were dominated by physiological noise and anatomical variability rather than imaging sequence differences. Even when changes in tSNR within subjects between MB 2 and 3 were considered there no clear reduction was seen with increasing MB factor (Figure 3) in these data. By using MB factor = 3 with sparse slice acquisition we were able to maintain whole-head coverage whilst obtaining a 2.25s MR quiet period, within our 3s TR, in which to study EEG-BOLD coupling. Therefore the relative gain in quiet period time far outweighed effects on tSNR which were encountered.

Benefits of MB fMRI for the simultaneous recording of high frequency EEG signals

The presence of residual GAs in EEG data at frequencies above 20 Hz shows the necessity of an MR quiet period to provide the best SNR for studying beta and gamma band signals. These residual artefacts are present despite strict adherence to best-current practice acquisition and the implementation of hardware solutions (synchronisation (Mandelkow et al., 2006; Mullinger et al., 2008) and optimal positioning (Mullinger et al., 2011)) and beamforming post-processing (Brookes et al., 2009, 2008) which are all designed to minimise the residual GAs. Whilst the magnitude of the residual GA appears to increase with frequency (Figure 6), it is actually relatively constant across the frequency bands above 20 Hz (Supporting Information, Figure S4c,d), but the relative contribution of the GA to the overall signal is increased due to the decrease in the amplitude of the underlying neuronal activity at higher frequencies resulting in Supporting Information, Figure S4e,f. These residual artefacts are likely to be caused by sub-

millimetre movements of the subject's head during data acquisition causing small changes in the GA profile, preventing perfect correction by template subtraction methods (Ritter et al., 2007; Yan et al., 2009). Given that such small head movements cannot be eliminated during acquisition and the current lack of a post-processing method to completely remove residual GAs from the EEG data, despite considerable effort by a number of groups (Brookes et al., 2008; Freyer et al., 2009; Maziero et al., 2016; Moosmann et al., 2009), the merit of an MR quiet period, that enables the study of higher frequency neuronal activity unadulterated by concurrent fMRI acquisition, is clear.

Indeed, using a sparse MR sequence incorporating quiet periods has previously been implemented to allow the study of gamma band activity during fMRI (Leicht et al., 2016; Mulert et al., 2010; Scheeringa et al., 2011). We have extended these previous works by showing that beta and gamma band activity from motor cortex can be measured in the MRI environment. We observed an ERS of gamma band power during the abduction movements compared with rest (Figs 5a and 6a&b) localised to cM1, in close agreement with previous MEG studies (Ball et al., 2008; Cheyne, 2013; Darvas et al., 2010; Muthukumaraswamy, 2010). This gamma band response was accompanied by a decrease (ERD) in beta band power (Figs 5b and 6c&d) which was observed in bilateral M1, in agreement with previous studies collected outside an MRI environment (Darvas et al., 2013; Jurkiewicz et al., 2006; Muthukumaraswamy et al., 2010). Interestingly, previous invasive and non-invasive electrophysiological recordings have shown that the gamma ERS is more spatially focal to cM1 than the beta ERD (Darvas et al., 2013; Miller et al., 2007), which was also observed in our data. In addition to the difference in the spatial localisation of the gamma/beta responses, we also observed different temporal profiles between the spectral responses from these locations. The gamma ERS covered a relatively large frequency range (~50-80Hz) and, whilst it could be

seen for the entire movement period, it was strongest at initial movement onset (i.e. 0-0.5s Fig 6a). The beta ERD was found to be much stronger and was present consistently throughout the entire movement period. Together these differences in spatial location and temporal response profile suggest different neuronal populations are driving these two responses, in line with previous findings (Darvas et al., 2010; Miller et al., 2007).

Given the considerable advantages of MRI for providing excellent spatial resolution of brain activity (De Martino et al., 2015; Heidemann et al., 2012) it is highly desirable to take advantage of this feature in the investigation of the origin of electrophysiological responses, where non-invasive EEG/MEG recordings are limited. However, previous studies (Leicht et al., 2016; Mulert et al., 2010; Scheeringa et al., 2011) have required considerable compromise on spatial resolution (slice thickness ranging from 4-8mm with slice gaps of 0.4-1mm) and/or brain coverage (between 35 and 120mm) to provide a sufficient quiet period to TR ratio (ranging between 30-90% of time) and sampling rate of MRI responses (TRs between 3 and 3.63s). With the current implementation of MB we have shown that these trade-offs can be minimised such that 3 mm isotropic voxels, with no slice gap and 99 mm brain coverage with a quiet period to TR ratio of 75%, can be achieved with a TR of 3s.

BOLD responses and coupling to EEG responses and future research possibilities

Exploiting the advantages of EEG-MB fMRI has allowed us to show the potential of this technique for non-invasively investigating brain function. We found that, out of all our regressors, the boxcar model of the finger abductions showed the strongest correlation with the BOLD response, with the largest activations arising in the contralateral postcentral gyrus (M1) [-38, -32, 66] mm, and supplementary motor area [-4, -14, 70] mm as well as bilateral S2. All

of which are regions expected to be activated in a simple sensorimotor task. Interestingly the regions of gamma-BOLD correlation were smaller and more focal, with peak activity being observed between the postcentral gyrus and superior parietal lobule both in contralateral [-32,-42, 60] mm, ipsilateral [34, -42, 60] mm regions, and a central peak found between precentral and postcentral gyrus at [2, -36, 56] mm. The contralateral activation extends to directly posterior to the hand-knob area of the left sensorimotor cortex, further suggesting this was a localised, task specific response. The bilaterality of this correlation, given the gamma ERS was lateralised to the left cM1, appears surprising, but falls consistently within the bilateral somatosensory cortex and therefore is likely to arise due to the mutual correlation of BOLD signals between the contralateral and ipsilateral regions of the somatosensory network for this task.

It is unsurprising given the robust task employed that the BOLD response was well characterised by a simple boxcar model and that this showed the strongest activations in the motor network. However, single-trial variability in BOLD and gamma ERS response amplitudes were well coupled in the somatosensory network. This finding supports previous work showing a tight coupling of natural variability in BOLD and gamma responses in the visual system (Logothetis, 2003; Scheeringa et al., 2011) and extends these findings into the sensorimotor modality. It is likely that the BOLD-gamma coupling was most evident in the sensory network where the variability to the task was the greatest and therefore least explained by the boxcar constant main effect. We hypothesize that a greater amount of response variability was elicited in the somatosensory network than the motor cortex as the subject's abduction movements showed such a high level of consistency in both timing and amplitude (Fig 4), reflecting similar motor output. However, it is possible that the sensation of finger movement, and thus the somatosensory input, may have varied depending on what external surfaces were touched with the finger when subjects' arms were slightly cramped for space

inside the scanner. Whilst this cannot be proven with these data, it provides a basis for further investigation.

The lack of significant correlation between the beta ERD and BOLD responses appears a surprising result given previous reports of negative beta-BOLD correlations (Ritter et al., 2009) and the clear beta band responses which we observed (Fig 5b). However, here we considered the variability in the EEG response which explained variance in the BOLD data in addition to that explained by a constant amplitude boxcar model. Further inspection of our data with a fixed effects cluster corrected Z>2.0 group analysis showed that beta-BOLD correlations were observed in central and ipsilateral motor cortex, but these did not survive mixed effects Z>2.3. Therefore it seems that the effect size was too weak for the beta correlation to arise in our data sample. Beta ERD is widely observed during preparation and execution of movements (Engel and Fries, 2010; Ritter et al., 2009; Zaepffel et al., 2013), however there is a sparsity of evidence directly linking parameters of the beta ERD amplitude to the quality of motor performance, leaving much still to be understood concerning beta oscillations precise functional role (Engel and Fries, 2010; Kilavik et al., 2013; Pogosyan et al., 2009). Given the beta ERD has been considered to be a simple gating mechanism (Fry et al., 2016; Stevenson et al., 2011) required to allow neuronal activity involved in task execution to take place in other, typically higher, frequency bands it is conceivable that the amplitude variability of the ERD is less related to the task performance and reflects more of a binarised signal to permit the necessary activation.

In conclusion we show that EEG can be safely acquired concurrently with GE-EPI MB-fMRI data and allows the investigation of neuronal and hemodynamic task responses with high

spatial, temporal and spectral resolution. We use a simple motor task in this work to show that tight gamma-BOLD coupling is observed on an individual trial basis, agreeing with previous invasive recordings in both animal and human visual/auditory cortex. In the future such methodologies that allow detailed integration of a wide frequency range of neural signals may be used to build a more complete understanding of pathways of feedforward and feedback neural communication and of how such signals contribute to neurovascular coupling mechanisms and the generation of the hemodynamic response.

Acknowledgements

We thank the Birmingham Nottingham Strategic Collaboration Fund for supporting this work and MU and a University of Nottingham Anne McLaren Fellowship for funding KJM and a University of Birmingham Fellowship for funding SDM.

References

Auerbach, E.J., Xu, J., Yacoub, E., Moeller, S., Ugurbil, K., 2013. Multiband accelerated spin-echo echo planar imaging with reduced peak RF power using time-shifted RF pulses. Magn Reson Med 69, 1261–1267. doi:10.1002/mrm.24719

Bagshaw, A.P., Aghakhani, Y., Bénar, C.G., Kobayashi, E., Hawco, C., Dubeau, F., Pike, G.B., Gotman, J., 2004. EEG-fMRI of focal epileptic spikes: Analysis with multiple haemodynamic functions and comparison with gadolinium-enhanced MR angiograms. Hum. Brain Mapp. 22, 179–192. doi:10.1002/hbm.20024

Ball, T., Demandt, E., Mutschler, I., Neitzel, E., Mehring, C., Vogt, K., Aertsen, A., Schulze-Bonhage, A., 2008. Movement related activity in the high gamma range of the human

EEG. Neuroimage 41, 302–310. doi:10.1016/j.neuroimage.2008.02.032

Bauer, M., Oostenveld, R., Peeters, M., Fries, P., 2006. Tactile spatial attention enhances gamma-band activity in somatosensory cortex and reduces low-frequency activity in parieto-occipital areas. J Neurosci 26, 490–501. doi:10.1523/JNEUROSCI.5228-04.2006

Becker, R., Reinacher, M., Freyer, F., Villringer, A., Ritter, P., 2011. How Ongoing Neuronal Oscillations Account for Evoked fMRI Variability. J. Neurosci. 31, 11016–11027. doi:10.1523/jneurosci.0210-11.2011

Bénar, C.G., Schön, D., Grimault, S., Nazarian, B., Burle, B., Roth, M., Badier, J.M., Marquis, P., Liegeois-Chauvel, C., Anton, J.L., 2007. Single-trial analysis of oddball event-related potentials in simultaneous EEG-fMRI. Hum. Brain Mapp. 28, 602–613. doi:10.1002/hbm.20289

Boorman, L., Harris, S., Bruyns-Haylett, M., Kennerley, A., Zheng, Y., Martin, C., Jones, M., Redgrave, P., Berwick, J., 2015. Long-Latency Reductions in Gamma Power Predict Hemodynamic Changes That Underlie the Negative BOLD Signal. J. Neurosci. 35, 4641–4656. doi:10.1523/JNEUROSCI.2339-14.2015

Boyacioğlu, R., Schulz, J., Koopmans, P.J., Barth, M., Norris, D.G., 2015. Improved sensitivity and specificity for resting state and task fMRI with multiband multi-echo EPI compared to multi-echo EPI at 7T. Neuroimage 119, 352–361. doi:10.1016/j.neuroimage.2015.06.089

Brookes, M.J., Mullinger, K.J., Stevenson, C.M., Morris, P.G., Bowtell, R., 2008. Simultaneous EEG source localisation and artifact rejection during concurrent fMRI by means of spatial filtering. Neuroimage 40, 1090–1104. doi:10.1016/j.neuroimage.2007.12.030

Brookes, M.J., Vrba, J., Mullinger, K.J., Geirsdottir, G.B., Yan, W.X., Stevenson, C.M., Bowtell, R., Morris, P.G., 2009. Source localisation in concurrent EEG/fMRI: applications at 7T. Neuroimage 45, 440–452. doi:S1053-8119(08)01160-9 [pii] 10.1016/j.neuroimage.2008.10.047

Brown, P., Salenius, S., Rothwell, J.C., Hari, R., 1998. Cortical correlate of the piper rhythm in humans. J. Neurophysiol. 80, 2911–2917.

Buschman, T.J., Miller, E.K., 2007. Top-down versus bottom-up control of attention in the prefrontal and posterior parietal cortices. Science 315, 1860–1862. doi:10.1126/science.1138071

Buzsaki, G., Draguhn, A., 2004. Neuronal Oscillations in Cortical Networks. Science (80-.). 304, 1926–1929. doi:10.1126/science.1099745

Carmichael, D.W., Thornton, J.S., Rodionov, R., Thornton, R., McEvoy, A., Allen, P.J., Lemieux, L., 2008. Safety of localizing epilepsy monitoring intracranial electroencephalograph electrodes using MRI: Radiofrequency-induced heating. J. Magn. Reson. Imaging 28, 1233–1244. doi:10.1002/jmri.21583

Castelhano, J., Duarte, I.C., Wibral, M., Rodriguez, E., Castelo-Branco, M., 2014. The dual facet of gamma oscillations: Separate visual and decision making circuits as revealed by simultaneous EEG/fMRI. Hum. Brain Mapp. 35, 5219–5235. doi:10.1002/hbm.22545

Chen, L., Vu, A.T., Xu, J., Moeller, S., Ugurbil, K., Yacoub, E., Feinberg, D.A., 2015. Evaluation of highly accelerated simultaneous multi-slice EPI for fMRI. Neuroimage 104, 452–459. doi:10.1016/j.neuroimage.2014.10.027

Cheyne, D., Bells, S., Ferrari, P., Gaetz, W., Bostan, A.C., 2008. Self-paced movements induce high-frequency gamma oscillations in primary motor cortex. Neuroimage 42,

332–342. doi:10.1016/j.neuroimage.2008.04.178

Cheyne, D., Ferrari, P., 2013. MEG studies of motor cortex gamma oscillations: evidence for a gamma "fingerprint" in the brain? Front. Hum. Neurosci. 7, 1–7. doi:10.3389/fnhum.2013.00575

Cheyne, D.O., 2013. MEG studies of sensorimotor rhythms: A review. Exp. Neurol. doi:10.1016/j.expneurol.2012.08.030

Colgin, L.L., Denninger, T., Fyhn, M., Hafting, T., Bonnevie, T., Jensen, O., Moser, M.-B., Moser, E.I., 2009. Frequency of gamma oscillations routes flow of information in the hippocampus. Nature 462, 353–357. doi:10.1038/nature08573

Collins, C.M., Wang, Z., 2011. Calculation of radiofrequency electromagnetic fields and their effects in MRI of human subjects. Magn. Reson. Med. 65, 1470–1482. doi:10.1002/mrm.22845

Crone, N.E., Miglioretti, D.L., Gordon, B., Lesser, R.P., 1998. Functional mapping of human sensorimotor cortex with electrocorticographic spectral analysis II. Event-related synchronization in the gamma band. Brain 121, 2301–2315. doi:10.1093/brain/121.12.2301

Darvas, F., Rao, R.P.N., Murias, M., 2013. Localized high gamma motor oscillations respond to perceived biologic motion. J. Clin. Neurophysiol. 30, 299–307. doi:10.1097/WNP.0b013e3182872f40

Darvas, F., Scherer, R., Ojemann, J.G., Rao, R.P., Miller, K.J., Sorensen, L.B., 2010. High gamma mapping using EEG. Neuroimage 49, 930–938. doi:10.1016/j.neuroimage.2009.08.041

De Martino, F., Moerel, M., Xu, J., Van De Moortele, P.F., Ugurbil, K., Goebel, R., Yacoub,

E., Formisano, E., 2015. High-resolution mapping of myeloarchitecture in vivo: Localization of auditory areas in the human brain. Cereb. Cortex 25, 3394–3405. doi:10.1093/cercor/bhu150

Debener, S., Ullsperger, M., Siegel, M., Engel, A.K., 2006. Single-trial EEG-fMRI reveals the dynamics of cognitive function. Trends Cogn. Sci. 10, 558–563. doi:10.1016/j.tics.2006.09.010

Debener, S., Ullsperger, M., Siegel, M., Fiehler, K., von Cramon, D.Y., Engel, A.K., 2005. Trial-by-trial coupling of concurrent electroencephalogram and functional magnetic resonance imaging identifies the dynamics of performance monitoring. J Neurosci 25, 11730–11737. doi:10.1523/JNEUROSCI.3286-05.2005

Delorme, A., Makeig, S., 2004. EEGLAB: an open source toolbox for analysis of single-trial EEG dynamics including independent component analysis. J Neurosci Methods 134, 9–21. doi:10.1016/j.jneumeth.2003.10.009 S0165027003003479 [pii]

Eichele, T., Calhoun, V.D., Moosmann, M., Specht, K., Jongsma, M.L.A., Quiroga, R.Q., Nordby, H., Hugdahl, K., 2008. Unmixing concurrent EEG-fMRI with parallel independent component analysis. Int. J. Psychophysiol. 67, 222–234. doi:10.1016/j.ijpsycho.2007.04.010

Eichele, T., Specht, K., Moosmann, M., Jongsma, M.L.A., Quiroga, R.Q., Nordby, H., Hugdahl, K., 2005. Assessing the spatiotemporal evolution of neuronal activation with single-trial event-related potentials and functional MRI. Proc Natl Acad Sci U S A 102, 17798–17803. doi:10.1073/pnas.0505508102

Engel, A.K., Fries, P., 2010. Beta-band oscillations-signalling the status quo? Curr. Opin. Neurobiol. doi:10.1016/j.conb.2010.02.015

Feinberg, D.A., Moeller, S., Smith, S.M., Auerbach, E., Ramanna, S., Gunther, M., Glasser, M.F., Miller, K.L., Ugurbil, K., Yacoub, E., 2010. Multiplexed echo planar imaging for sub-second whole brain FMRI and fast diffusion imaging. PLoS One 5, e15710. doi:10.1371/journal.pone.0015710

Feinberg, D.A., Setsompop, K., 2013. Ultra-fast MRI of the human brain with simultaneous multi-slice imaging. J. Magn. Reson. doi:10.1016/j.jmr.2013.02.002

Fell, J., Klaver, P., Lehnertz, K., Grunwald, T., Schaller, C., Elger, C.E., Fernandez, G., 2001. Human memory formation is accompanied by rhinal-hippocampal coupling and decoupling. Nat. Neurosci. 4, 1259–1264. doi:10.1038/nn759

Foged, M.T., Lindberg, U., Vakamudi, K., Larsson, H.B.W., Pinborg, L.H., Kjñr, T.W., Fabricius, M., Svarer, C., Ozenne, B., Thomsen, C., Beniczky, S., Paulson, O.B., Posse, S., 2017. Safety and EEG data quality of concurrent high-density EEG and high-speed fMRI at 3 Tesla. PLoS One 12. doi:10.1371/journal.pone.0178409

Freyer, F., Becker, R., Anami, K., Curio, G., Villringer, A., Ritter, P., 2009. Ultrahigh-frequency EEG during fMRI: Pushing the limits of imaging-artifact correction. Neuroimage 48, 94–108. doi:10.1016/j.neuroimage.2009.06.022

Fries, P., 2009. Neuronal gamma-band synchronization as a fundamental process in cortical computation. Annu Rev Neurosci 32, 209–224. doi:10.1146/annurev.neuro.051508.135603

Fry, A., Mullinger, K.J., O'Neill, G.C., Barratt, E.L., Morris, P.G., Bauer, M., Folland, J.P., Brookes, M.J., 2016. Modulation of post-movement beta rebound by contraction force and rate of force development. Hum. Brain Mapp. 37, 2493–2511. doi:10.1002/hbm.23189

Gaetz, W., MacDonald, M., Cheyne, D., Snead, O.C., 2010. Neuromagnetic imaging of movement-related cortical oscillations in children and adults: Age predicts post-movement beta rebound. Neuroimage 51, 792–807. doi:10.1016/j.neuroimage.2010.01.077

Goldman, R.I., Stern, J.M., Engel Jerome, J., Cohen, M.S., 2002. Simultaneous EEG and fMRI of the alpha rhythm. Neuroreport 13, 2487–2492. doi:10.1097/01.wnr.0000047685.08940.d0

Goldman, R.I., Wei, C.Y., Philiastides, M.G., Gerson, A.D., Friedman, D., Brown, T.R., Sajda, P., 2009. Single-trial discrimination for integrating simultaneous EEG and fMRI: identifying cortical areas contributing to trial-to-trial variability in the auditory oddball task. Neuroimage 47, 136–147. doi:10.1016/j.neuroimage.2009.03.062

Green, J.J., Boehler, C.N., Roberts, K.C., Chen, L.-C., Krebs, R.M., Song, A.W., Woldorff, M.G., 2017. Cortical and Subcortical Coordination of Visual Spatial Attention Revealed by Simultaneous EEG–fMRI Recording. J. Neurosci. 37, 7803–7810. doi:10.1523/JNEUROSCI.0326-17.2017

Hall, S.D., Holliday, I.E., Hillebrand, A., Singh, K.D., Furlong, P.L., Hadjipapas, A., Barnes, G.R., 2005. The missing link: Analogous human and primate cortical gamma oscillations. Neuroimage 26, 13–17. doi:10.1016/j.neuroimage.2005.01.009

Heidemann, R.M., Ivanov, D., Trampel, R., Fasano, F., Meyer, H., Pfeuffer, J., Turner, R., 2012. Isotropic submillimeter fMRI in the human brain at 7 T: combining reduced field-of-view imaging and partially parallel acquisitions. Magn Reson Med 68, 1506–1516. doi:10.1002/mrm.24156

Hermes, D., Miller, K.J., Wandell, B. a, Winawer, J., 2014. Stimulus Dependence of Gamma Oscillations in Human Visual Cortex. Cereb. Cortex 1–9. doi:10.1093/cercor/bhu091

Hillebrand, A., Barnes, G.R., 2005. Beamformer Analysis of MEG Data. Int. Rev. Neurobiol. doi:10.1016/S0074-7742(05)68006-3

Hoogenboom, N., Schoffelen, J.M., Oostenveld, R., Fries, P., 2010. Visually induced gamma-band activity predicts speed of change detection in humans. Neuroimage 51, 1162–1167. doi:10.1016/j.neuroimage.2010.03.041

Hoogenboom, N., Schoffelen, J.M., Oostenveld, R., Parkes, L.M., Fries, P., 2006. Localizing human visual gamma-band activity in frequency, time and space. Neuroimage 29, 764–773. doi:10.1016/j.neuroimage.2005.08.043

Horovitz, S.G., Fukunaga, M., De Zwart, J.A., Van Gelderen, P., Fulton, S.C., Balkin, T.J., Duyn, J.H., 2008. Low frequency BOLD fluctuations during resting wakefulness and light sleep: A simultaneous EEG-fMRI study. Hum. Brain Mapp. 29, 671–682. doi:10.1002/hbm.20428

Howard, M.W., Rizzuto, D.S., Caplan, J.B., Madsen, J.R., Lisman, J., Aschenbrenner-Scheibe, R., Schulze-Bonhage, A., Kahana, M.J., 2003. Gamma Oscillations Correlate with Working Memory Load in Humans. Cereb. Cortex 13, 1369–1374. doi:10.1093/cercor/bhg084

Huster, R.J., Debener, S., Eichele, T., Herrmann, C.S., 2012. Methods for simultaneous EEG-fMRI: an introductory review. J Neurosci 32, 6053–6060. doi:10.1523/JNEUROSCI.0447-12.2012

Jung, T.P., Makeig, S., Westerfield, M., Townsend, J., Courchesne, E., Sejnowski, T.J., 2000. Removal of eye activity artifacts from visual event-related potentials in normal and clinical subjects. Clin Neurophysiol 111, 1745–1758. doi:S1388-2457(00)00386-2 [pii]

Jurkiewicz, M.T., Gaetz, W., Bostan, A.C., Cheyne, D., 2006. Post-movement beta rebound

is generated in motor cortex: Evidence from neuromagnetic recordings. Neuroimage 32, 1281–1289.

Kilavik, B.E., Zaepffel, M., Brovelli, A., MacKay, W.A., Riehle, A., 2013. The ups and downs of beta oscillations in sensorimotor cortex. Exp. Neurol. doi:10.1016/j.expneurol.2012.09.014

Laufs, H., Kleinschmidt, A., Beyerle, A., Eger, E., Salek-Haddadi, A., Preibisch, C., Krakow, K., 2003. EEG-correlated fMRI of human alpha activity. Neuroimage 19, 1463–1476.

Leicht, G., Vauth, S., Polomac, N., Andreou, C., Rauh, J., Mu??mann, M., Karow, A., Mulert, C., 2016. EEG-Informed fMRI Reveals a Disturbed Gamma-Band-Specific Network in Subjects at High Risk for Psychosis. Schizophr. Bull. 42, 239–249. doi:10.1093/schbul/sbv092

Logothetis, N.K., 2008. What we can do and what we cannot do with fMRI. Nature 453, 869–878. doi:10.1038/nature06976

Logothetis, N.K., 2003. The underpinnings of the BOLD functional magnetic resonance imaging signal. J Neurosci 23, 3963–3971.

Logothetis, N.K., Pauls, J., Augath, M., Trinath, T., Oeltermann, A., 2001. Neurophysiological investigation of the basis of the fMRI signal. Nature 412, 150–157. doi:10.1038/35084005

Magri, C., Schridde, U., Murayama, Y., Panzeri, S., Logothetis, N.K., 2012. The amplitude and timing of the BOLD signal reflects the relationship between local field potential power at different frequencies. J Neurosci 32, 1395–1407. doi:32/4/1395 [pii] 10.1523/JNEUROSCI.3985-11.2012

Mandelkow, H., Halder, P., Boesiger, P., Brandeis, D., 2006. Synchronization facilitates

removal of MRI artefacts from concurrent EEG recordings and increases usable bandwidth. Neuroimage 32, 1120–1126. doi:10.1016/j.neuroimage.2006.04.231

Mantini, D., Perrucci, M.G., Del Gratta, C., Romani, G.L., Corbetta, M., 2007. Electrophysiological signatures of resting state networks in the human brain. Proc Natl Acad Sci U S A 104, 13170–13175. doi:10.1073/pnas.0700668104

Mayhew, S.D., Dirckx, S.G., Niazy, R.K., Iannetti, G.D., Wise, R.G., 2010. EEG signatures of auditory activity correlate with simultaneously recorded fMRI responses in humans. Neuroimage 49, 849–864. doi:10.1016/j.neuroimage.2009.06.080

Mayhew, S.D., Li, S., Kourtzi, Z., 2012. Learning acts on distinct processes for visual form perception in the human brain. J. Neurosci. 32, 775–86. doi:10.1523/JNEUROSCI.2033-11.2012

Mayhew, S.D., Ostwald, D., Porcaro, C., Bagshaw, A.P., 2013. Spontaneous EEG alpha oscillation interacts with positive and negative BOLD responses in the visual-auditory cortices and default-mode network. Neuroimage 76, 362–372. doi:10.1016/j.neuroimage.2013.02.070

Maziero, D., Velasco, T.R., Hunt, N., Payne, E., Lemieux, L., Salmon, C.E.G., Carmichael, D.W., 2016. Towards motion insensitive EEG-fMRI: Correcting motion-induced voltages and gradient artefact instability in EEG using an fMRI prospective motion correction (PMC) system. Neuroimage 138, 13–27. doi:10.1016/j.neuroimage.2016.05.003

Medicines and Healthcare Products Regulatory Agency, 2015. Safety Guidelines for Magnetic Resonance Imaging Equipment in Clinical Use.

Michels, L., Bucher, K., Lüchinger, R., Klaver, P., Martin, E., Jeanmonod, D., Brandeis, D.,

2010. Simultaneous EEG-fMRI during a working memory task: Modulations in low and high frequency bands. PLoS One 5, 1–15. doi:10.1371/journal.pone.0010298

Miller, K.J., Leuthardt, E.C., Schalk, G., Rao, R.P.N., Anderson, N.R., Moran, D.W., Miller, J.W., Ojemann, J.G., 2007. Spectral Changes in Cortical Surface Potentials during Motor Movement. J. Neurosci. 27, 2424–2432. doi:10.1523/JNEUROSCI.3886-06.2007

Mobascher, A., Brinkmeyer, J., Warbrick, T., Musso, F., Wittsack, H.J., Saleh, A., Schnitzler, A., Winterer, G., 2009. Laser-evoked potential P2 single-trial amplitudes covary with the fMRI BOLD response in the medial pain system and interconnected subcortical structures. Neuroimage 45, 917–926. doi:10.1016/j.neuroimage.2008.12.051

Moeller, S., Yacoub, E., Olman, C.A., Auerbach, E., Strupp, J., Harel, N., Ugurbil, K., 2010. Multiband multislice GE-EPI at 7 tesla, with 16-fold acceleration using partial parallel imaging with application to high spatial and temporal whole-brain fMRI. Magn Reson Med 63, 1144–1153. doi:10.1002/mrm.22361

Moosmann, M., Schönfelder, V.H., Specht, K., Scheeringa, R., Nordby, H., Hugdahl, K., 2009. Realignment parameter-informed artefact correction for simultaneous EEG-fMRI recordings. Neuroimage 45, 1144–1150. doi:10.1016/j.neuroimage.2009.01.024

Mukamel, R., Gelbard, H., Arieli, A., Hasson, U., Fried, I., Malach, R., 2005. Coupling between neuronal firing, field potentials, and FMRI in human auditory cortex. Science 309, 951–954. doi:10.1126/science.1110913

Mulert, C., Leicht, G., Hepp, P., Kirsch, V., Karch, S., Pogarell, O., Reiser, M., Hegerl, U., Jäger, L., Moller, H.J., McCarley, R.W., 2010. Single-trial coupling of the gamma-band response and the corresponding BOLD signal. Neuroimage 49, 2238–2247. doi:10.1016/j.neuroimage.2009.10.058

Mullinger, K.J., Bowtell, R., 2011. Combining EEG and FMRI. Methods Mol. Biol. 711, 303–326.

Mullinger, K.J., Debener, S., Coxon, R., Bowtell, R., 2008a. Effects of simultaneous EEG recording on MRI data quality at 1.5, 3 and 7 tesla. Int. J. Psychophysiol. 67, 178–188. doi:10.1016/j.ijpsycho.2007.06.008

Mullinger, K.J., Mayhew, S.D., Bagshaw, A.P., Bowtell, R., Francis, S.T., 2014. Evidence that the negative BOLD response is neuronal in origin: a simultaneous EEG-BOLD-CBF study in humans. Neuroimage 94, 263–274.

Mullinger, K.J., Mayhew, S.D., Bagshaw, A.P., Bowtell, R., Francis, S.T., 2013. Poststimulus undershoots in cerebral blood flow and BOLD fMRI responses are modulated by poststimulus neuronal activity. Proc Natl Acad Sci U S A 110, 13636–13641. doi:10.1073/pnas.1221287110

Mullinger, K.J., Morgan, P.S., Bowtell, R.W., 2008b. Improved artifact correction for combined electroencephalography/functional MRI by means of synchronization and use of vectorcardiogram recordings. J Magn Reson Imaging 27, 607–616. doi:10.1002/jmri.21277

Mullinger, K.J., Yan, W.X., Bowtell, R., 2011. Reducing the gradient artefact in simultaneous EEG-fMRI by adjusting the subject's axial position. Neuroimage 54, 1942–1950. doi:S1053-8119(10)01281-4 [pii] 10.1016/j.neuroimage.2010.09.079

Murta, T., Hu, L., Tierney, T.M., Chaudhary, U.J., Walker, M.C., Carmichael, D.W., Figueiredo, P., Lemieux, L., 2016. A study of the electro-haemodynamic coupling using simultaneously acquired intracranial EEG and fMRI data in humans. Neuroimage 142, 371–380. doi:10.1016/j.neuroimage.2016.08.001

Muthukumaraswamy, S.D., 2013. High-frequency brain activity and muscle artifacts in MEG/EEG: a review and recommendations. Front. Hum. Neurosci. 7, 1–11. doi:10.3389/fnhum.2013.00138

Muthukumaraswamy, S.D., 2010. Functional Properties of Human Primary Motor Cortex Gamma Oscillations. J. Neurophysiol. 104, 2873–2885. doi:10.1152/jn.00607.2010

Muthukumaraswamy, S.D., Edden, R.A.E., Jones, D.K., Swettenham, J.B., Singh, K.D., 2009. Resting GABA concentration predicts peak gamma frequency and fMRI amplitude in response to visual stimulation in humans. Proc Natl Acad Sci U S A 106, 8356–8361. doi:10.1073/pnas.0900728106

Muthukumaraswamy, S.D., Singh, K.D., 2013. Visual gamma oscillations: The effects of stimulus type, visual field coverage and stimulus motion on MEG and EEG recordings. Neuroimage 69, 223–230. doi:10.1016/j.neuroimage.2012.12.038

Muthukumaraswamy, S.D., Singh, K.D., Swettenham, J.B., Jones, D.K., 2010. Visual gamma oscillations and evoked responses: variability, repeatability and structural MRI correlates. Neuroimage 49, 3349–3357. doi:10.1016/j.neuroimage.2009.11.045

Niessing J, Ebisch B, Schmidt K, Niessing M, Singer W, Galuske R, 2005. Hemodynamic Signals Correlate Tightly with Synchronized Gamma Oscillations. Science (80-.). 309, 948–951. doi:10.1126/science.1110948

Nir, Y., Fisch, L., Mukamel, R., Gelbard-Sagiv, H., Arieli, A., Fried, I., Malach, R., 2007. Coupling between Neuronal Firing Rate, Gamma LFP, and BOLD fMRI Is Related to Interneuronal Correlations. Curr. Biol. 17, 1275–1285. doi:10.1016/j.cub.2007.06.066

Norris, D.G., Koopmans, P.J., Boyacio??lu, R., Barth, M., 2011. Power independent of number of slices (PINS) radiofrequency pulses for low-power simultaneous multislice

excitation. Magn. Reson. Med. 66, 1234–1240. doi:10.1002/mrm.23152

Novitskiy, N., Ramautar, J.R., Vanderperren, K., De Vos, M., Mennes, M., Mijovic, B., Vanrumste, B., Stiers, P., Van den Bergh, B., Lagae, L., Sunaert, S., Van Huffel, S., Wagemans, J., 2011. The BOLD correlates of the visual P1 and N1 in single-trial analysis of simultaneous EEG-fMRI recordings during a spatial detection task. Neuroimage 54, 824–835. doi:10.1016/j.neuroimage.2010.09.041

Olafsson, V., Kundu, P., Wong, E.C., Bandettini, P.A., Liu, T.T., 2015. Enhanced identification of BOLD-like components with multi-echo simultaneous multi-slice (MESMS) fMRI and multi-echo ICA. Neuroimage. doi:10.1016/j.neuroimage.2015.02.052

Olbrich, S., Mulert, C., Karch, S., Trenner, M., Leicht, G., Pogarell, O., Hegerl, U., 2009. EEG-vigilance and BOLD effect during simultaneous EEG/fMRI measurement. Neuroimage 45, 319–332. doi:10.1016/j.neuroimage.2008.11.014

Oostenveld, R., Fries, P., Maris, E., Schoffelen, J.M., 2011. FieldTrip: Open source software for advanced analysis of MEG, EEG, and invasive electrophysiological data. Comput Intell Neurosci 2011, 156869. doi:10.1155/2011/156869

Pantev, C., Makeig, S., Hoke, M., Galambos, R., Hampson, S., Gallen, C., 1991. Human auditory evoked gamma-band magnetic fields. Proc. Natl. Acad. Sci. U. S. A. 88, 8996–9000. doi:10.1073/pnas.88.20.8996

Pogosyan, A., Gaynor, L.D., Eusebio, A., Brown, P., 2009. Boosting Cortical Activity at Beta-Band Frequencies Slows Movement in Humans. Curr. Biol. 19, 1637–1641. doi:10.1016/j.cub.2009.07.074

Ritter, P., Becker, R., Graefe, C., Villringer, A., 2007. Evaluating gradient artifact correction

of EEG data acquired simultaneously with fMRI. Magn. Reson. Imaging 25, 923–932. doi:10.1016/j.mri.2007.03.005

Ritter, P., Moosmann, M., Villringer, A., 2009. Rolandic alpha and beta EEG rhythms' strengths are inversely related to fMRI-BOLD signal in primary somatosensory and motor cortex. Hum Brain Mapp 30, 1168–1187. doi:10.1002/hbm.20585

Robinson, S.E., Vrba, J., 1999. Functional neuroimaging by synthetic aperture magnetometry (SAM). Recent Adv. Biomagn. Tohoku Uni, 302–305.

Rosa, M.J., Kilner, J., Blankenburg, F., Josephs, O., Penny, W., 2010. Estimating the transfer function from neuronal activity to BOLD using simultaneous EEG-fMRI. Neuroimage 49, 1496–1509. doi:10.1016/j.neuroimage.2009.09.011

Schadow, J., Lenz, D., Dettler, N., Fründ, I., Herrmann, C.S., 2009. NeuroImage Early gamma-band responses re fl ect anticipatory top-down modulation in the auditory cortex. Neuroimage 47, 651–658. doi:10.1016/j.neuroimage.2009.04.074

Scheeringa, R., Fries, P., Petersson, K.-M., Oostenveld, R., Grothe, I., Norris, D.G., Hagoort, P., Bastiaansen, M.C.M., 2011. Neuronal Dynamics Underlying High- and Low-Frequency EEG Oscillations Contribute Independently to the Human BOLD Signal. Neuron 69, 572–583. doi:10.1016/j.neuron.2010.11.044

Scheibe, C., Ullsperger, M., Sommer, W., Heekeren, H.R., 2010. Effects of parametrical and trial-to-trial variation in prior probability processing revealed by simultaneous electroencephalogram/functional magnetic resonance imaging. J Neurosci 30, 16709–16717. doi:30/49/16709 [pii] 10.1523/JNEUROSCI.3949-09.2010

Schoffelen, J., Oostenveld, R., Fries, P., 2005. Neuronal coherence as a mechanism of effective corticospinal interaction. Science 308, 111–113. doi:10.1126/science.1107027

Scholvinck, M.L., Maier, A., Ye, F.Q., Duyn, J.H., Leopold, D.A., 2010. Neural basis of global resting-state fMRI activity. Proc Natl Acad Sci U S A 107, 10238–10243. doi:0913110107 [pii] 10.1073/pnas.0913110107

Singer, W., Gray, C.M., 1995. Visual Feature Integration and the Temporal Correlation Hypothesis. Annu. Rev. Neurosci. 18, 555–586. doi:10.1146/annurev.neuro.18.1.555

Stevenson, C.M., Brookes, M.J., Morris, P.G., 2011. β-Band correlates of the fMRI BOLD response. Hum. Brain Mapp. 32, 182–197. doi:10.1002/hbm.21016

Sumiyoshi, A., Suzuki, H., Ogawa, T., Riera, J.J., Shimokawa, H., Kawashima, R., 2012. Coupling between gamma oscillation and fMRI signal in the rat somatosensory cortex: Its dependence on systemic physiological parameters. Neuroimage 60, 738–746. doi:10.1016/j.neuroimage.2011.12.082

Todd, N., Moeller, S., Auerbach, E.J., Yacoub, E., Flandin, G., Weiskopf, N., 2016. Evaluation of 2D multiband EPI imaging for high-resolution, whole-brain, task-based fMRI studies at 3T: Sensitivity and slice leakage artifacts. Neuroimage 124, 32–42. doi:10.1016/j.neuroimage.2015.08.056

van Drongelen, W., Yuchtman, M., Van Veen, B., van Huffelen, A., 1996. A spatial filtering technique to detect and localize multiple sources in the brain. Brain Topogr. 9, 39–49.

van Veen, B.D., van Drongelen, W., Yuchtman, M., Suzuki, A., 1997. Localization of brain electrical activity via linearly constrained minimum variance spatial filtering. Biomedical 44, 867–880. doi:10.1109/10.623056

Viswanathan, A., Freeman, R.D., 2007. Neurometabolic coupling in cerebral cortex reflects synaptic more than spiking activity. Nat Neurosci 10, 1308–1312. doi:10.1038/nn1977

Winawer, J., Kay, K.N., Foster, B.L., Rauschecker, A.M., Parvizi, J., Wandell, B.A., 2013.

Asynchronous Broadband Signals Are the Principal Source of the BOLD Response in Human Visual Cortex. Curr. Biol. 23, 1145–1153. doi:10.1016/j.cub.2013.05.001

Womelsdorf, T., Fries, P., Mitra, P.P., Desimone, R., 2006. Gamma-band synchronization in visual cortex predicts speed of change detection. Nature 439, 733–736. doi:10.1038/nature04258

Wong, E., 2012. Optimized phase schedules for minimizing peak RF power in simultaneous multi-slice RF excitation pulses, in: Proceedings of the 20th Annual Meeting of ISMRM. Melbourne, Australia, p. 2209.

Woolrich, M.W., Behrens, T.E., Beckmann, C.F., Jenkinson, M., Smith, S.M., 2004. Multilevel linear modelling for FMRI group analysis using Bayesian inference. Neuroimage 21, 1732–1747. doi:10.1016/j.neuroimage.2003.12.023 S1053811903007894 [pii]

Yan, W.X., Mullinger, K.J., Brookes, M.J., Bowtell, R., 2009. Understanding gradient artefacts in simultaneous EEG/fMRI. Neuroimage 46, 459–471.

Yan, W.X., Mullinger, K.J., Geirsdottir, G.B., Bowtell, R., 2010. Physical modeling of pulse artefact sources in simultaneous EEG/fMRI. Hum Brain Mapp 31, 604–620. doi:10.1002/hbm.20891

Zaepffel, M., Trachel, R., Kilavik, B.E., Brochier, T., 2013. Modulations of EEG Beta Power during Planning and Execution of Grasping Movements. PLoS One 8, 1–10. doi:10.1371/journal.pone.0060060

Zhang, Y., Brady, M., Smith, S., 2001. Segmentation of brain MR images through a hidden Markov random field model and the expectation-maximization algorithm. IEEE Trans Med Imaging 20, 45–57. doi:10.1109/42.906424

Figures & Tables

Table 1. Mean temporal SNR (tSNR) (±standard deviation) calculated over grey matter across 3 participants during five MR sequences: MB: 1-3; acquisition type = equidistant or sparse. All other parameters were constant: TR/TE=3060/40ms, SENSE=2, slices=36, FA=79°, Volumes=41.

Multiband Factor	Slice acquisition spacing	tSNR
1	Equidistant	74 ± 40
2	Equidistant	72 ± 39
2	Sparse	67 ± 37
3	Equidistant	68 ± 37
3	Sparse	74 ± 38

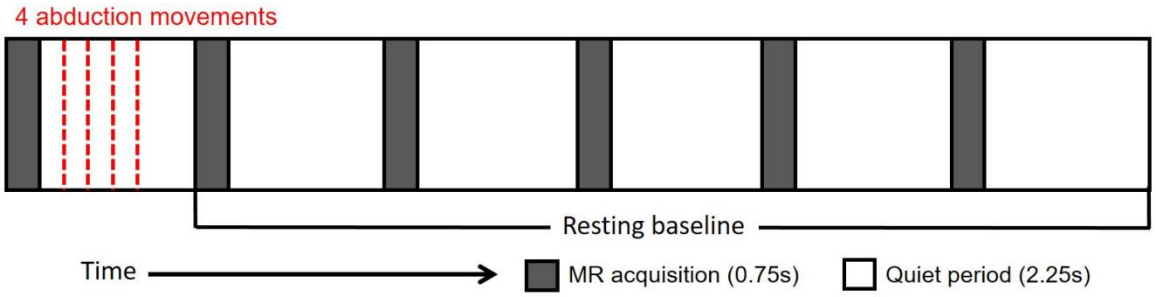

Figure 1. Schematic of the sparse MB=3 fMRI scanning scheme and the motor task paradigm showing when four abduction movements were performed within the MR gradient quiet period of a single volume, and were followed by a 16s resting baseline interval for each trial. This results in the movements being performed every 18s.

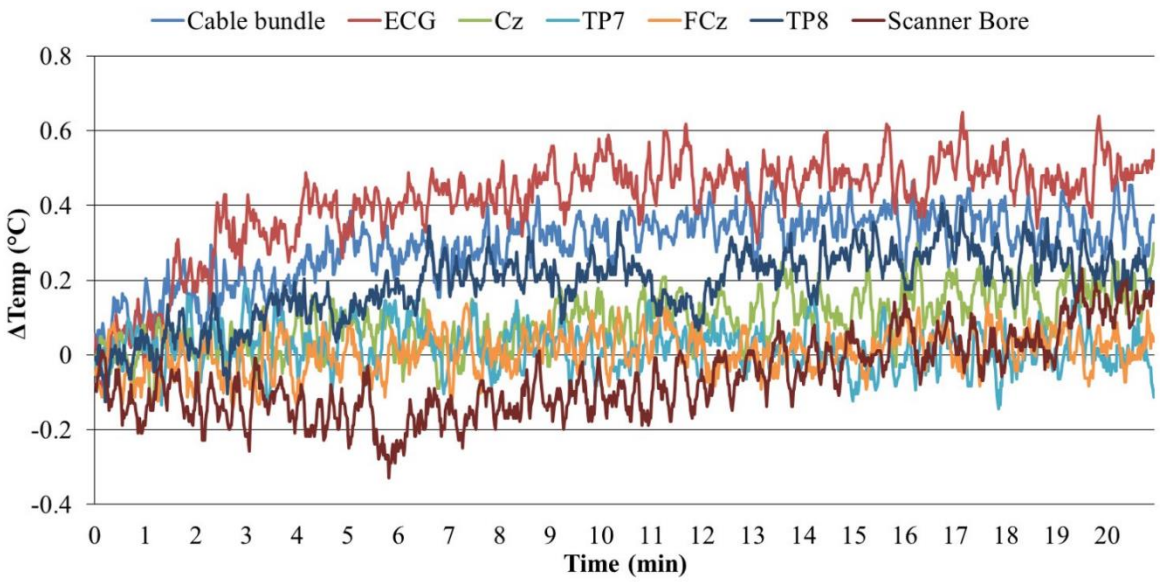

Figure 2. Temperature changes at EEG electrodes, cable bundle and a control location on the scanner bore during a 20-minute GE-EPI sequence scan (MB factor = 4, TR/TE=1000/40 ms, SENSE=2, slices=48, B1 RMS=1.09μT, SAR/head=22%) using a Philips Achieva 3T MRI scanner. Temperature was calculated relative to an initial 5-minute baseline recording made before the scan started.

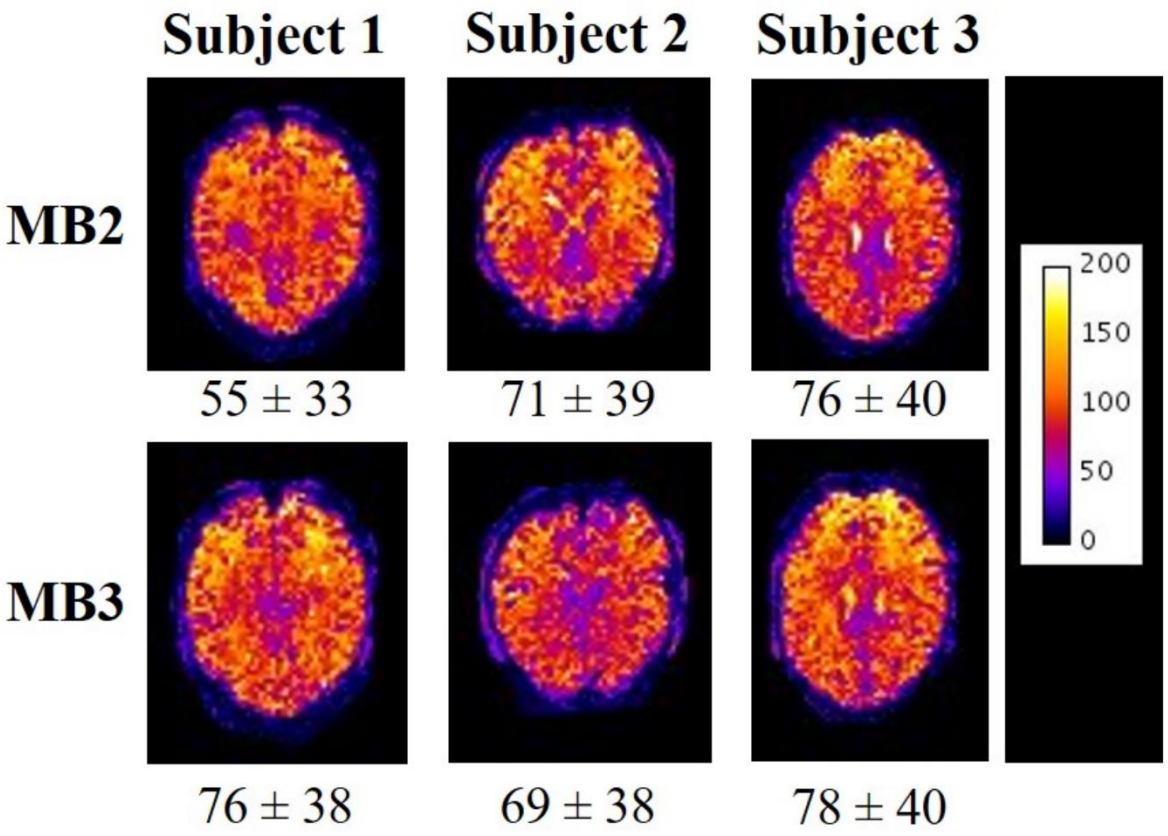

Figure 3. Spatial maps of tSNR of middle slice of the stack for each subject for sparse image acquisition sequences with MB factor 2 (top row) and 3 (bottom row). The values below the each map show the mean tSNR ± SD over all grey matter voxels for a given subject and scan.

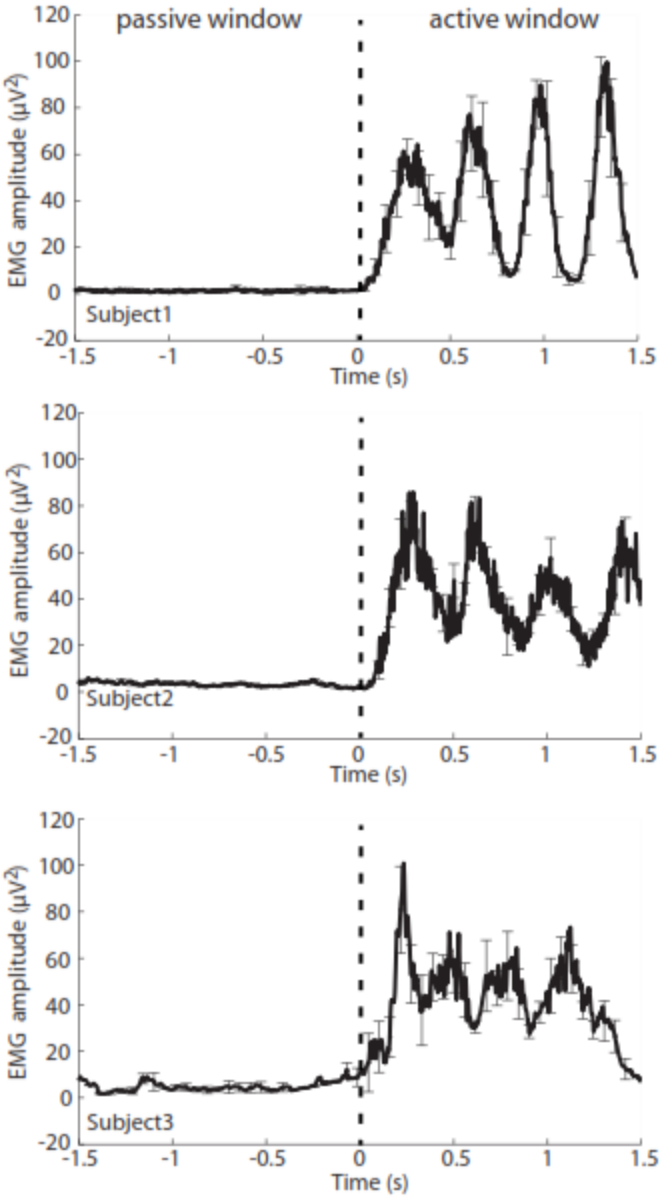

Figure 4. EMG activity recorded from the right FDI during the passive (-9 to -7.5s) and active (0-1.5s) time windows (here the time windows are concatenated together for visualisation purposes) from three representative subjects. The average timecourse across all trials and runs from a representative subject is shown. Onset of the first auditory cue occurred at 0s relative to index finger abduction movements. Error bars denote standard deviation across runs.

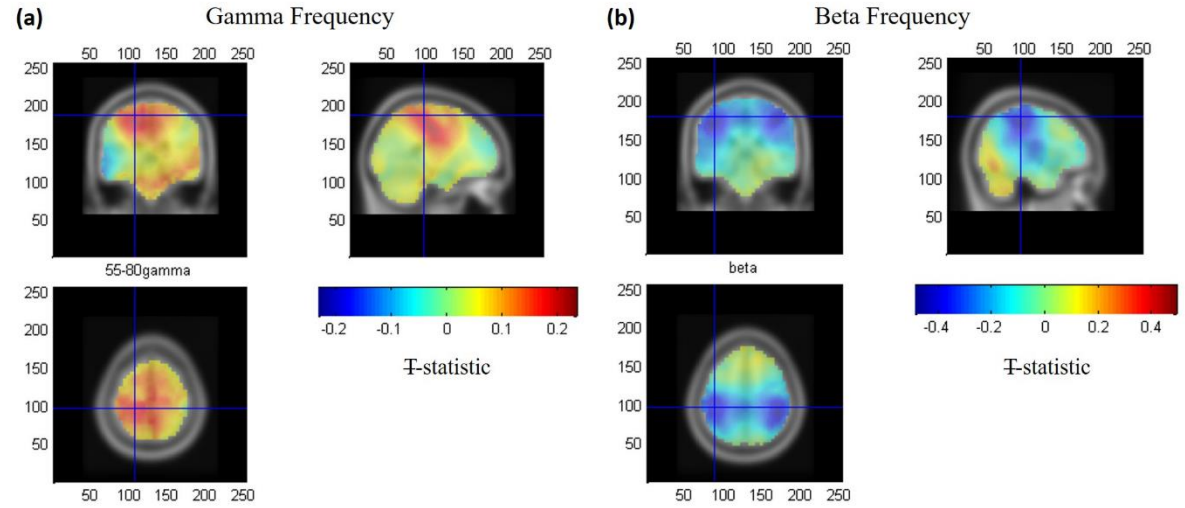

Figure 5. Group average (N=10) T-statistic beamformer maps showing regions exhibiting power increases and decreases in **a)** gamma- and **b)** beta-power, respectively, during the active window (0-1.5s) as compared with the passive window (-9.5-7s). The crosshairs represent the group average of the individual VE locations found in cM1 for the gamma (**a**) and beta (**b**) frequency activity.

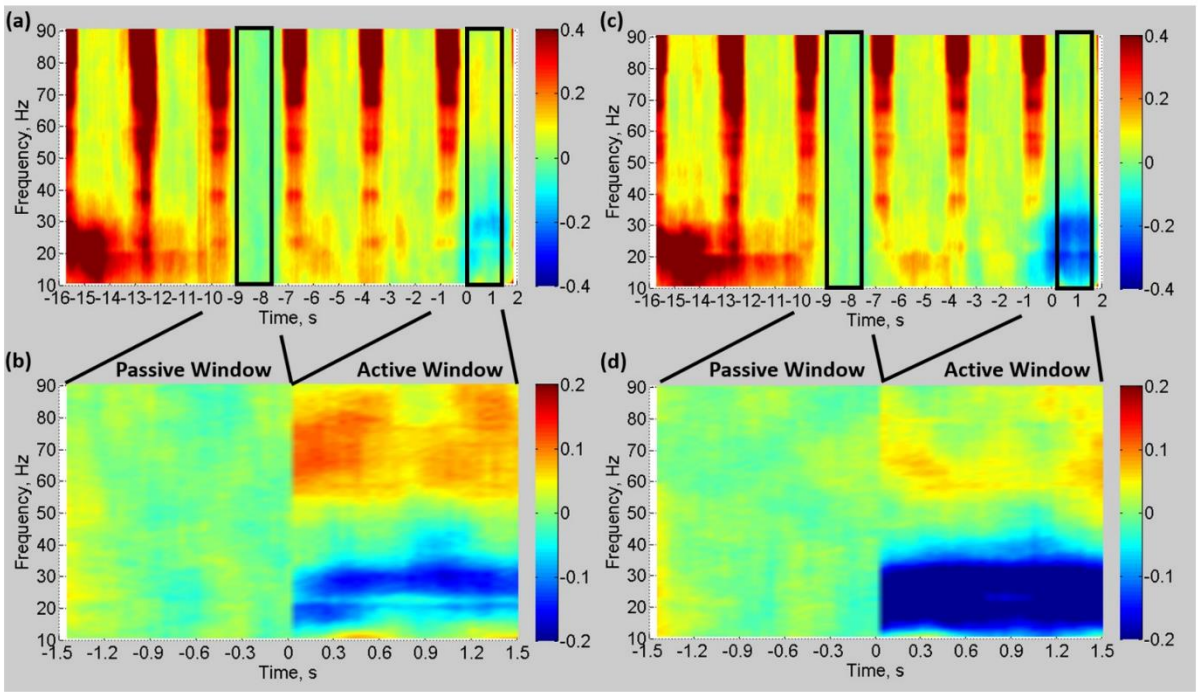

Figure 6. Group mean (N=10) time-frequency spectrograms demonstrating changes in the EEG signal power in cM1 relative to the passive window (-9 to -7.5s) for **a&b)** gamma ERS

and **c&d)** beta ERD VE location. The passive window was located in an MR quiet period and before any anticipation of the stimulus. Time is displayed relative to the auditory cue onset. Spectrograms were calculated with frequency resolution of 2.5Hz with spectral smoothing of ±10Hz. **a&c)** show 18s whole-trial duration, note the residual GAs during fMRI acquisition periods. **b&d)** show the gamma and beta power responses during the active window (0 to 1.5s) where movement occurred, with the passive window data appended pre-stimulus for comparison. Colour bars denote the relative change in power from the average power during the passive window period (baseline measure) of the passive window for each frequency. See Supporting Information, Figure S4 for absolute power changes of same time-frequency spectrograms.

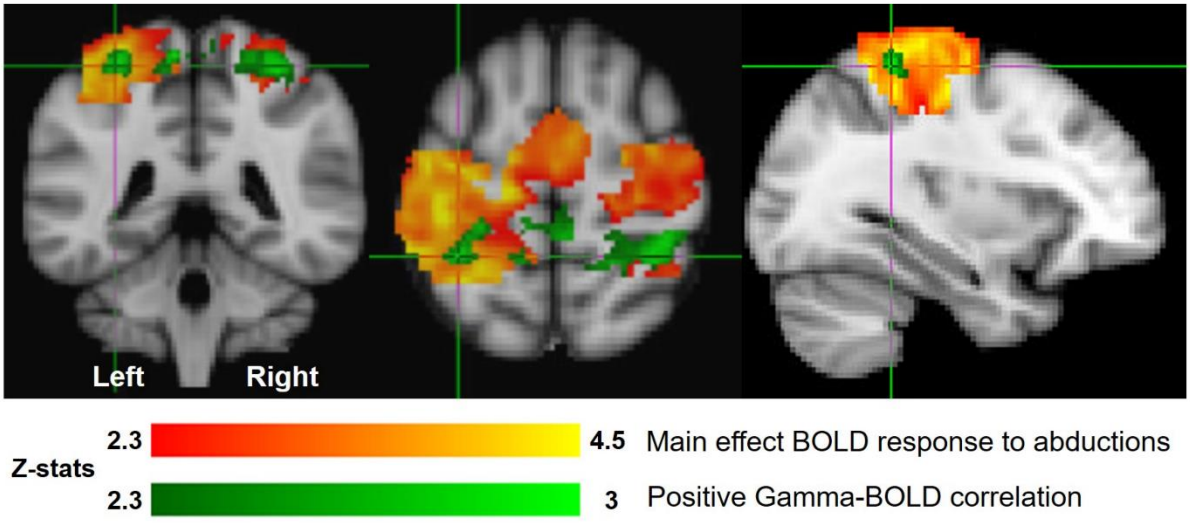

Figure 7. Group average (N=10) fMRI mixed effects results. Positive correlation of BOLD signal to the boxcar model of right index finger abduction movements (red-yellow) and areas of positive gamma-BOLD correlation (green). All correlations are cluster corrected with $p < 0.05$, masked with motor cortex. The crosshairs represent the peak positive gamma-BOLD correlation in cM1 (at [-32, -42, 60] mm).

Supporting Information

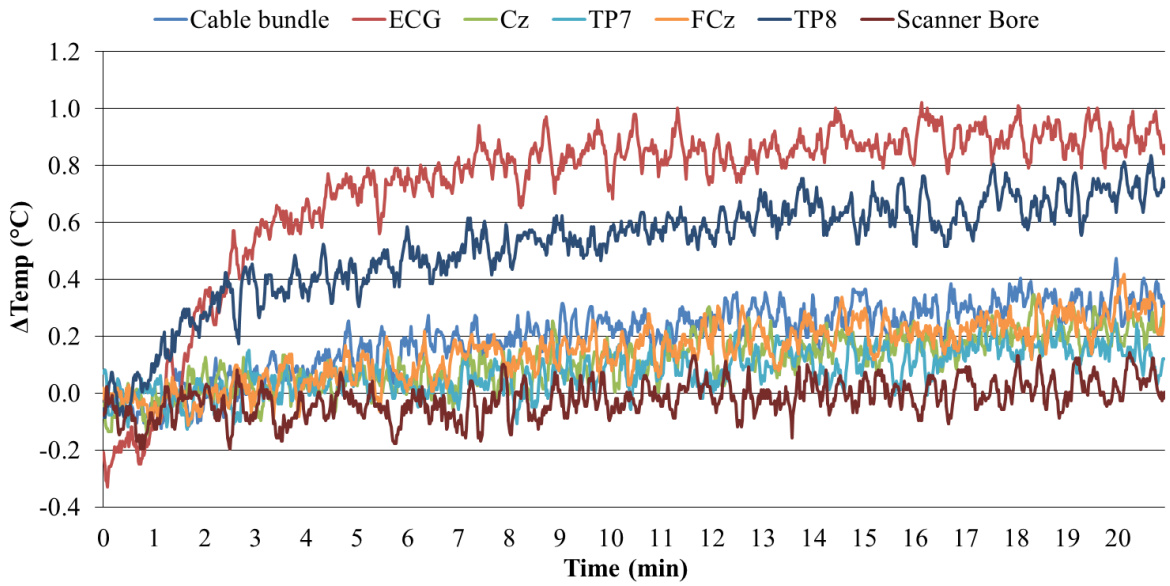

Figure S1. Temperature changes at EEG electrodes, cable bundle and a control location on the scanner bore during a 20-minute PCASL-GE-EPI sequence scan (Multiband factor = 4, TR/TE=3500/9.8ms, SENSE=2, slices=32, B1 RMS=1.58μT, SAR/head=46%) using a Philips Achieva 3T MRI scanner. Temperature was calculated relative to an initial 5-minute baseline recording made before the scan.

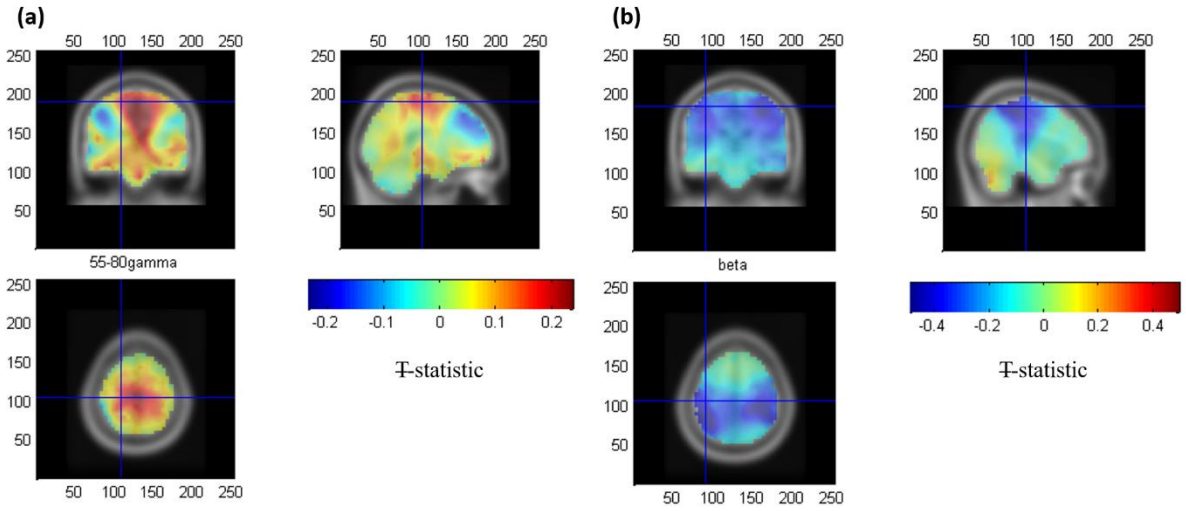

Figure S2. Group average (N=10) T-statistic beamformer maps calculated from the data recorded outside the scanner. Maps show regions exhibiting power increases and decreases in **a)** gamma- and **b)** beta-power, respectively, during the active window (0-1.5s) as compared with the passive window (-9.5-7s). The crosshairs represent the group average of the individual VE locations found in cM1 for the gamma (**a**) and beta (**b**) frequency activity.

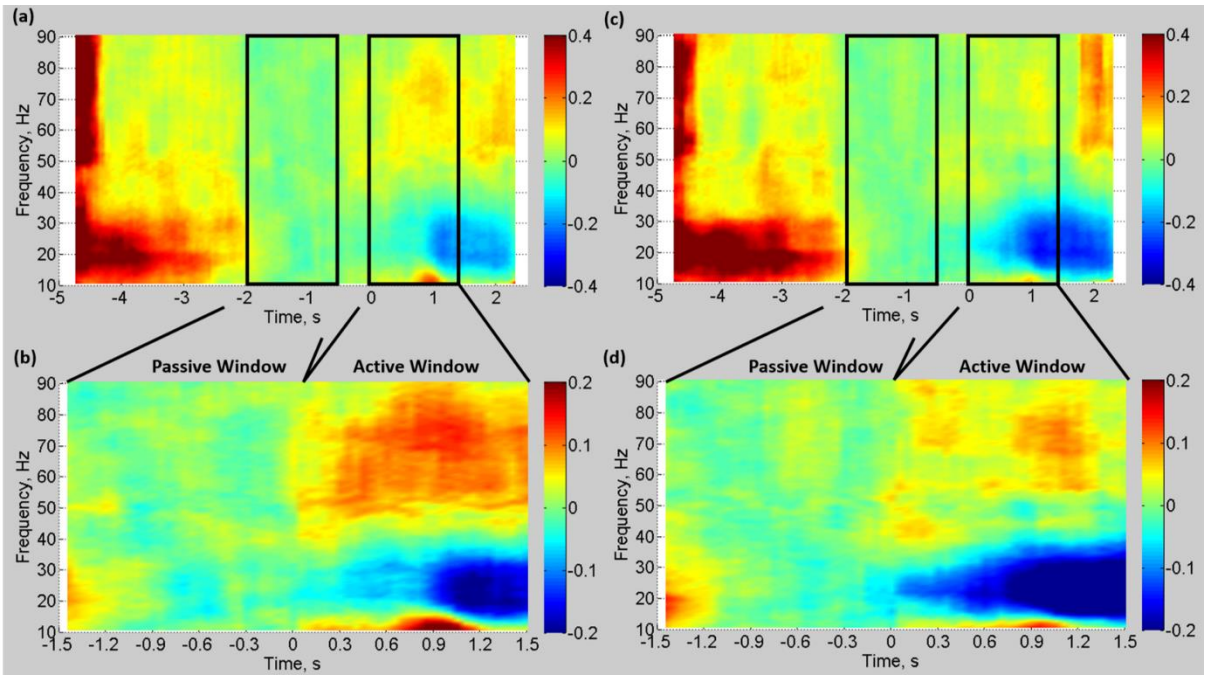

Figure S3. Group mean (N=10) time-frequency spectrograms calculated from data recorded outside of the scanner. Spectrograms demonstrate changes in the EEG signal power in cM1 relative to the passive window (-2 to -0.5s) for **a&b)** gamma ERS and **c&d)** beta ERD VE location. Time is displayed relative to the auditory cue onset. Spectrograms were calculated with frequency resolution of 2.5Hz with spectral smoothing of ±10Hz. **a&c)** show 7s whole-trial duration, **b&d)** show the gamma and beta power responses during the active window (0 to 1.5s) where movement occurred, with the passive window data appended pre-stimulus for comparison. Colour bars denote the relative change in power from the average power during the passive window period (baseline measure) of the passive window for each frequency.

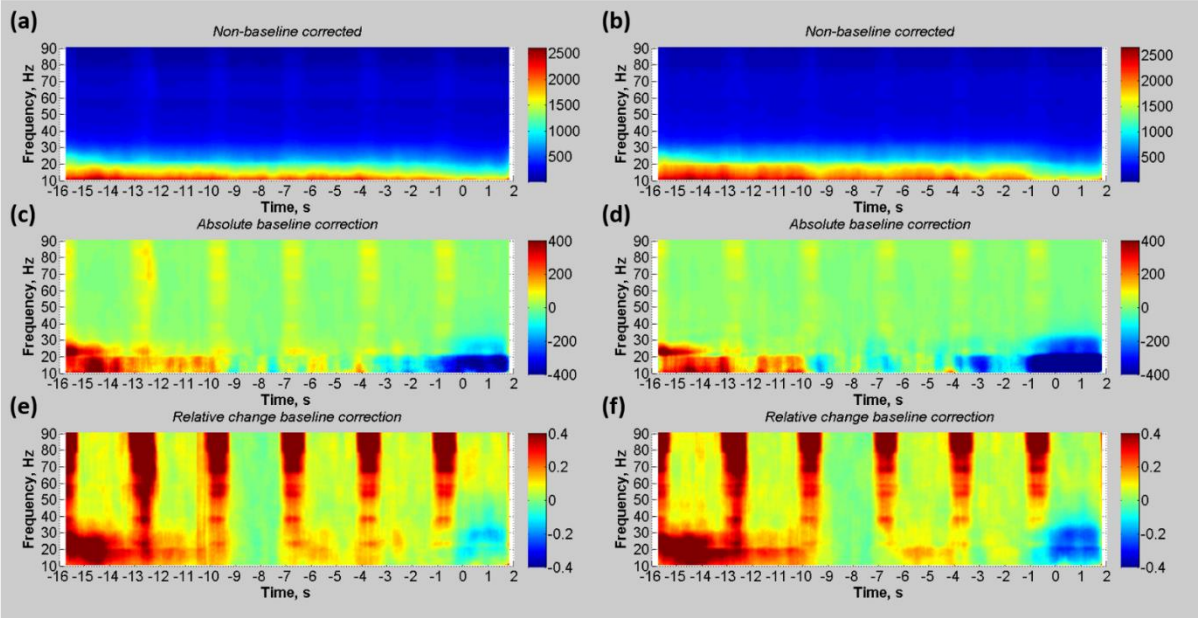

Figure S4. Group mean (N=10) time-frequency spectrograms calculated from data recorded inside of the scanner during fMRI. Spectrograms demonstrate changes in the EEG signal power from contralateral primary motor cortex for **a&c&e)** gamma ERS and **b&d&f)** beta ERD VE location. The passive window (-9 to -7.5s), used for baseline correction, was located in an MR quiet period and before any anticipation of the stimulus. Time is displayed relative to the auditory cue onset. Spectrograms calculated with frequency resolution of 2.5Hz with spectral smoothing of ±10Hz. **a&b)** show non-baseline corrected values. **c&d)** show the absolute baseline corrected values which were calculated by subtracting mean baseline power calculated from the average of the passive window for each frequency. **e&f)** show the relative change baseline corrected values which was calculated by dividing the absolute baseline corrected values by baseline value for each frequency, and used in Figure 6.